FLOW REVERSAL EVENTS AND STATISTICAL MODELING OF FLOW DYNAMICS OF HYPERSALINE WATER ACROSS A CONSTRUCTED CAUSEWAY, GREAT SALT LAKE, UTAH, USA

by

Michael Lawrence Freeman

A thesis submitted to the faculty of
The University of Utah
in partial fulfillment of the requirements for the degree of

Master of Science

Department of Geography

The University of Utah

August 2014

The University of Utah Graduate School

STATEMENT OF THESIS APPROVAL

The thesis of **Michael Lawrence Freeman**

has been approved by the following supervisory committee members:

Kathleen Nicoll	, Chair	**April 18, 2014** Date Approved
Simon Brewer	, Member	**April 18, 2014** Date Approved
David Naftz	, Member	**April 18, 2014** Date Approved

and by **Andrea Brunelle** , Chair/Dean of

the Department/College/School of **Geography**

and by David B. Kieda, Dean of The Graduate School.

ABSTRACT

The hypersaline Great Salt Lake (GSL), located in the western United States, is divided into a north arm (Gunnison Bay) and a south arm (Gilbert Bay) by a 29-km earth-filled railroad causeway completed in 1959. Flow between the two bays is restricted to an 88-m wide breach at the western end of the causeway known as the GSL Breach. A gauging station at the GSL Breach monitors flow across the causeway. Flow across the GSL Breach is dynamic, ranging from -166 m^3/s to 340 m^3/s over the 5-year analysis period (2009-2013). The prominent flow direction is from south-to-north reported as positive discharge and flow from north-to-south is reported as negative discharge. Negative discharge events at the GSL Breach are referred to as flow reversal events (FRE). During the 5-year period of analysis, a total of 1510 FRE were recorded at the GSL Breach gauging station, with an average of 302 events occurring each year. Several FREs were short in duration, lasting 15-minutes or less. The longest event recorded at the GSL Breach was 1950-minutes (32.5 hours). FRE are most common when the difference between the water surface elevations of Gilbert and Gunnison Bay is at a minimum (September through December). Longer duration FRE are most common during the cool seasons (September to May) when large storm systems cross over the GSL Basin. To determine the variables influencing discharge and FREs at the GSL Breach, we applied several predictor variables to a generalized additive model (GAMs). GAMs were used to develop an effective predictive model for discharge at the GSL Breach using smoothing

functions of predictor variables measured at various hydrologic and meteorological stations. We assessed the use of GAMs for accurate prediction of discharge by statistical analysis, residual plots, and time-series analysis using observed daily values at the GSL Breach gauging station. Models using wind gust, wind direction, lake elevation, and stream stage as predictor variables produce valid explanatory results for discharge at the GSL Breach. GAMs proved to be an effective method for capturing the rapid changes in discharge observed at the GSL Breach, suggesting the sensitivity of the GAM is of sufficient resolution for understanding the hydrodynamics of the GSL. To improve model accuracy, additional lake level monitoring equipment should be installed on the north and south side of the causeway and a weather station at the center of the GSL causeway is needed.

CONTENTS

ABSTRACT iii

LIST OF FIGURES vii

LIST OF TABLES ix

ACKNOWLEDGEMENTS x

1. INTRODUCTION 1

2. BACKGROUND 7

2.1 Great Salt Lake Regional Significance 7
2.2 Great Salt Lake Causeway and Breach 8
2.3 Great Salt Lake Water Surface Elevation 9
2.4 Great Salt Lake Hydrologic Flow Monitoring 13

3. METHODOLOGY 16

3.1 Meteorological Datasets 16
3.2 Hydrological Data Collection 16
3.3 Hydrologic Datasets 17
3.4 Palmer Drought Severity Index 18
3.5 Flow Reversal Event Evaluation 18
3.6 Generalized Additive Model 19
3.7 Cross-Validation of Generalized Additive Model 20

4. RESULTS AND DISCUSSION 22

4.1 Flow Reversal Events Summary 22
4.2 Case Study of Flow Reversal Event: April 27-28, 2010 29
4.3 Generalized Additive Model 34
4.3.1 Generalized Additive Model Development 34
4.3.2 Generalized Additive Model Prediction 38
4.3.3 Cross-Validation 48
4.4 Generalized Additive Model Interpretation 48
4.4.1 Smoothed Term Plots 48

4.4.2 Predictive Discharge Contour Maps..... 52
4.4.2.1 Lake Elevation Discharge Contour Maps ……..…56
4.4.2.2 Wind Direction and Magnitude Discharge Contour Maps ……58
4.5 Generalized Additive Model Limitation and Improvements..... 61
4.6 Generalized Additive Model Implications..... 63

5. CONCLUSIONS..... 65

6. REFERENCES 70

LIST OF FIGURES

1. Location of GSL causeway, stream gauging stations, lake elevation gauges, and the Hat Island and Promontory Point weather stations, Great Salt Lake…..……..…10

2. Great Salt Lake historic elevation record and elevations during the 5-year study period…….……...……...12

3. Time-series analysis of a FRE occurring on April 8-9, 2013…..……..…..24

4. Frequency of FRE and the average duration of FRE occurring at the GSL Breach gauging station from 2009 to 2013…….…….25

5. Mean daily lake water surface elevations measured at the Saltair and Saline Lake gauging stations showing the fluctuations in water surface elevations between Gilbert and Gunnison bays in 2009……..…27

6. Time-series analysis of the FRE on April 27-28, 2010……..……..…30

7. Cross-sectional schematic showing the displacement of water within Gilbert and Gunnison bays as a result of a southern wind event over the GSL…….....31

8. Cross-sectional schematic showing the displacement of water within Gilbert and Gunnison bays as a result of a northern wind event over the GSL……..……...…33

9. Residual plots with corresponding root mean square error values of mean daily discharge values from models GH7-GH10 and observed mean daily discharge at the GSL Breach…….....….40

10. Residual plots with corresponding root mean square error values of mean daily discharge values from models GP7-GP10 and observed mean daily discharge at the GSL Breach…….....….41

11. Time-series analysis of mean daily discharge values observed at the GSL Breach and predicted values using models GH7, GH8, GP7, and GP8…….43

12. Time-series analysis of mean daily discharge values observed at the GSL Breach and predicted values using models GH9, GH10, GP9, and GP10 ...……...……..….44

13. Lake elevation of Gilbert and Gunnison Bay for water year 2009-2013 with monthly Palmer Drought Severity Index for the GSL Basin ……....47

14. Cross-validation residual plots with corresponding root mean square error values of modeled mean daily discharge values and observed mean daily discharge at the GSL Breach…….……..……49

15. Smoothed term plots of predictor variables applied to model GH10……..…51

16. Predictive discharge contour map demonstrating how lake water surface elevation at Saltair and Saline influence the magnitude of discharge at the GSL Breach……..53

17. Predictive discharge contour map demonstrating how wind speed and wind direction influence the magnitude and flow direction of discharge at the GSL Breach…….....54

18. Predictive discharge contour map demonstrating how wind speed and wind direction influence the magnitude and flow direction of discharge at the GSL Breach during a FRE……..…55

LIST OF TABLES

1. Hydrologic and meteorological station information for explanatory variables collected for GAM analysis……...…….. 14

2. Model identification number, variables, and statistical summaries of GAMs…..... 21

3. Summary of FREs recorded at the GSL Breach gauging station from October 1, 2008 to September 30, 2013…….. 23

4. GSL Breach stage, Saltair lake water surface elevation, and corresponding cross-sectional area measured at the GSL Breach gauging station……. 59

ACKNOWLEDGEMENTS

This study was made possible in part due to the data made available by the governmental agencies, commercial firms, and educational institutions participating in the University of Utah MesoWest and the USGS stream-gauging networks. I would like to personally thank my thesis committee members Kathleen Nicoll, David Naftz, and Simon Brewer for their help and support with this work. Special thanks to all my friends and family for all your support and encouragement over the last two years. Thank you, Ashley, my beautiful wife, for all your love, support, and encouragement during this process. I could not have done it without you.

1. INTRODUCTION

Natural and constructed structures that partition a water body can significantly affect local hydrologic processes and the exchange of water, salt, and nutrients. Inlets, harbors, and breaches are important exchange points between adjoining water bodies. The hydrodynamics at these points are influenced by chemical and physical variables, including density stratification (e.g., salinity and water temperature), meteorological forces (e.g., wind and pressure), and tidal cycles. Improved instrumentation, hydroacoustic methods, and the application of statistical and numerical models have advanced the study of water transport, circulation, and chemical loading potential across these structures. Some recent hydrodynamic studies have assessed water exchange (Ghezzo et al., 2010; Hamblin and He, 2003; MacCready et al., 2009; Ström and Klaveness, 2003), density driven flow (Jia and Li, 2012a; Jia and Li, 2012b), stratified flow (Ferrarin and Umgiesser, 2005; Gianni et al., 2011; Gianni and Zacharias, 2012; Zacharias and Gianni, 2008; Zemlys et al., 2013), and flow reversals (Beal et al., 2000; Elken et al., 2003; Ilicak et al., 2008; Smeed, 1997; Smeed, 2004). Such emerging technical approaches have strong potential to facilitate impact assessment in watersheds, and can inform strategic planning, abatement of anthropogenic activities, and the design of built structures to minimize environmental effects.

The Aral Sea in central Asia, Urmia Lake in northwestern Iran, and the Great Salt Lake (GSL) in the western USA are three large hypersaline water bodies located in arid

desert landscape settings that are vulnerable to natural hydroclimatic variations (e.g., floods, drought) and the consequences of anthropogenic activities (e.g., water extractions, input diversions, earthwork constructions, etc.). These water bodies are presently partitioned, creating distinctive hydrologic processes relative to the exchange of water and its associated solutes.

The rapid decline of water levels in the Aral Sea and its subsequent desertification over the past 50+ years has been reported in the popular press and scientific literature. As a result of declining water levels from 1987-1989, the South Aral Sea became separated into an East and West Lobe, which are connected by the incised Kulandy Channel (Zavialov et al., 2009). Density driven flow exchange has been observed during the spring and early summer (Roget et al., 2009; Zavialov et al., 2009). Hydrographic investigations have verified that discharge in the Kulandy Channel is affected by meteorological factors, including sustained winds and wind direction, which increase water velocities and circulation within the channel (Roget et al., 2009; Zavialov et al., 2003; Zavialov et al., 2009). These meteorologically influenced flow events have been linked to increased mixing of brine within the two lobes of the Aral Sea, and erosion within the Kulandy Channel (Zavialov et al., 2009).

Urmia Lake is partitioned by a causeway to support the Shahid Kalantari highway, which was constructed between 1979 and 1994 (Marjani and Jamali, 2014). The 15 km causeway divides Urmia Lake into a north and south lake connected by a 1250-m wide opening in the causeway (Marjani and Jamali, 2014; Zeinoddini et al., 2009). More than 95 percent of the freshwater enters Urmia Lake south of the causeway, affecting the water and salinity distribution of the lake (Marjani and Jamali, 2014;

Zeinoddini et al., 2009). The south lake is less saline than the north lake, leading to two-layer bidirectional flow through the causeway opening, causing the less saline waters of the south lake to flow over the more saline waters of the north lake (Marjani and Jamali, 2014). Numerical modeling by Marjani and Jamali (2014) and Zeinoddini et al. (2009) assessed the effects of the causeway structure on the salinity and water balance between the north and south lakes. The primary variables influencing the discharge across the causeway opening and exchange of brine and water between the two partitions include seasonal freshwater inputs to the south lake, wind direction, and wind speed (Marjani and Jamali, 2014).

Much like the Aral Sea and Urmia Lake, the GSL is a partitioned water body that is hydrologically influenced by meteorological factors. Similar to Urmia Lake, the GSL is partitioned by a rock-filled causeway constructed for a railroad that separates the lake into a north arm, known as Gunnison Bay, and a south arm, called Gilbert Bay (Gwynn, 2002). Gilbert Bay receives approximately 95 percent of the freshwater input to GSL, whereas Gunnison Bay receives only 5 percent of the freshwater input (Loving et al., 2000). Depending on freshwater inflows to GSL, the salinity of Gilbert and Gunnison bays varies, with salinities ranging from 50 to 170 ppt in Gilbert Bay and salinity ranging from 150 to 270 ppt in Gunnison Bay (Utah Division of Forestry, Fire and State Lands, 2012). Prior to 2014, the causeway structure contained two 4.6-m wide by 6.1-m deep box culverts (East and West Culverts) and an 88-m opening in the causeway referred to as the GSL Breach. These three openings within the causeway have limited exchange of water and brine between the two arms of the GSL (Gwynn, 2002; Loving et al., 2000)

Beginning in 2012, the western culvert of the causeway was filled; more recently

in December of 2013, the eastern culvert was filled, confining the majority of water and brine exchange between the two bays to the GSL Breach (Associated Press, 2013; Jacobs Associates, 2013; Maffly, 2013a; Maffly, 2013b; Maffly, 2013c; Union Pacific Railroad, 2013). Recent proposals are in place to construct a new railroad causeway breach to increase circulation between the two bays (Associated Press, 2013; Jacobs Associates, 2013; Maffly, 2013a; Maffly, 2013b; Maffly, 2013c; Union Pacific Railroad, 2013). These planned modifications and future changes to the causeway structure will affect water and salt exchange between Gilbert and Gunnison Bay, requiring significant updates to the existing water and salt balance models derived for the GSL (Gwynn, 2002; Hahl and Handy, 1969; Loving et al., 2000; Madison, 1970; Waddell and Bolke, 1973; Waddell and Fields, 1977; Wold et al., 1997).

Specific variables influencing flow at the GSL Breach have not been described in detail. To better contextualize water exchange across the GSL Breach, we have assessed the real-time discharge record at the GSL Breach published by the U.S. Geological Survey (USGS) over a 5-year timeframe (water year (WY) 2009-2013). We used the data measured at the GSL Breach to characterize flow events across the causeway opening. Using the time-series data, we examined, in detail, specific flow reversal events (FRE) (north-to-south) that have occurred during the 5-year study period to understand additional spatiotemporal controls on hydrologic gradient (or head difference) and lake elevation. Time-series analysis identified meteorological and hydrological variables influencing discharge across the breach. We then used the meteorological and hydrological variables to statistically model discharge at the GSL Breach.

To evaluate the nonlinear relationship between the hydrologic and meteorological

variables affecting discharge at the GSL Breach, we used a Generalized Additive Model (GAM) to predict discharge at the GSL Breach. A GAM (Hastie and Tibshirani, 1990; Wood, 2006) is a generalized linear model (GLM) (McCullagh and Nelder, 1989) that applies smoothing functions to additive nonlinear predictor variables. The smoothing functions allow the data to shape the relationship between the predictor and response variables. GAMs are referred to as data-driven statistical models, as the model is defined by the relationship between the set of predictor variables and the response variable (Guisan et al., 2002; Hastie and Tibshirani, 1990; Wood, 2006). GAMs are versatile modeling frameworks for systems that have nonlinear relationships between response and predictor variables. The application of GAMs has been successful in a variety of studies, including hydrological modeling (Asquith et al., 2013), ecological modeling (Augustin et al., 1998; Guisan et al., 2002), water quality monitoring (Morton and Henderson, 2008), precipitation trends (Underwood, 2009), and hydrologic drought forecasting (Wen et al., 2011). Using the GAM method, we tested the variables affecting discharge at the GSL Breach and the hypothesis that strength (magnitude), duration, and direction of wind events affect lake elevation of the two bays at the GSL, which influences the magnitude and direction of flow across the GSL Breach.

This paper will: 1) introduce the GSL regional setting and hydrologic data collection; 2) present observations about the frequency, duration, and seasonality of FREs observed at the GSL Breach; 2) present a case study describing a FRE at the GSL Breach; 3) discuss the application of a generalized additive model (GAM) to the GSL hydrologic setting to assess the key predictor variables for determining discharge at the GSL Breach; 3) relate the methods and results of a GAM analysis application using time-series data

derived from local meteorological and hydrologic gauging stations; and 4) compare modeled results with published discharge values collected at the GSL Breach.

2. BACKGROUND

2.1 Great Salt Lake Regional Significance

The GSL is a nontidal terminal meromictic lake located in the Great Basin Physiographic Province, which is endorheic (internally-drained). The GSL is the largest saline water body in the United States, and is the fourth largest terminal lake in the world, with a surface area that can exceed 5,100 km^2 (Naftz et al., 2009). The lake is shallow, with an average depth of 4.3 meters at an average water surface elevation of 1280.2 meters (Utah Division of Forestry, Fire and State Lands, 2012). The GSL open water area and surrounding wetlands are one of the largest refuges for shorebirds and migratory waterfowl in the western hemisphere (Aldrich and Paul, 2002). Similar to Urmia Lake, waterfowl feed on the abundant brine shrimp populations (Artemia franciscana) that inhabit the waters of GSL (Wurtsbaugh and Maciej Gliwicz, 2001). Industry also utilizes the GSL ecosystem. The harvesting of brine shrimp cysts for aquaculture and mineral extraction from evaporation ponds along the shores of the GSL are lucrative extractive industries. The combination of industry and tourism of the lake generates an estimated $1.3 billion dollar economy to the State of Utah (Bioeconomics Inc., 2012). The economic importance of the GSL ecosystem has increased awareness and management decisions regarding the operation and utilization of the lake's resources.

2.2 Great Salt Lake Causeway and Breach

Prior to 1959, the GSL was a homogenous, well-mixed body of water (Wold et al., 1997). In 1959, the Southern Pacific Transportation Company constructed a rock-filled railroad causeway spanning 29 km across the GSL (Gwynn, 2002), which partitioned the lake into Gilbert and Gunnison bays. After completion of the causeway, circulation of water between the two bays was limited to the locations of two box culverts. The disruption of lake-wide circulation has caused an imbalance of water and salt because approximately 95 percent of freshwater inputs to the GSL basin enter the lake south of the causeway via the Weber, Bear, and Jordan Rivers (Loving et al., 2000) resulting in salinization of the north arm (Arnow and Stephens, 1990) and a higher lake water surface elevation of the south arm creating a hydrologic head gradient (Loving et al., 2000). To control rapidly rising lake levels in 1982-84, the GSL Breach (88-m in length) was opened in 1984 along the western end of the causeway near Lakeside, UT (Gwynn, 2002; Loving et al., 2000). The GSL Breach reduced the lake elevation in Gilbert Bay, which alleviated flooding along the southern shores of GLS and increased circulation of water and brine between Gilbert and Gunnison bays (Loving et al., 2000).

The construction of the GSL Breach allowed water and brine to flow from both south-to-north and north-to-south, creating two layers of flow separated by an interface layer. The two layers of flow are commonly referred to as bidirectional flow at the GSL Breach and previously at the GSL culverts. Flow from south-to-north is driven by the higher water-surface elevation of Gilbert Bay. South-to-north flow is observed at the surface above the interface layer. Flow from north-to-south is driven by a density gradient between Gunnison and Gilbert Bay. The dense brine of Gunnison Bay flows

into Gilbert Bay by diving under the less saline waters of Gilbert Bay. The water density gradient moves dense brine of Gunnison Bay into the deeper bathymetry of GSL located within Gilbert Bay. The north-to-south flow is observed below the interface layer.

Receding lake levels during the early 1990s and 2000s resulted in diminished circulation between Gilbert and Gunnison bays. Routine dredging of the GSL Breach was employed to maintain circulation between the two bays as lake levels decreased (Gwynn, 2002; Gwynn, 2012; Loving et al., 2000). In 2003, the GSL Breach was dredged to its current channel depth of 1278 m (Gwynn, 2012). Due to shallow bathymetry (1278 m) at the Breach, flow from north-to-south is infrequent when lake water surface elevations are lower than 1280 m, which is the modern lake elevation threshold for bidirectional flow at the GSL Breach. USGS discharge measurements indicate that bidirectional flow has not occurred at the GSL Breach since 2003.

2.3 Great Salt Lake Water Surface Elevation

Since 1847, the USGS has measured lake water surface elevation of the GSL (U.S. Geological Survey, 2013a). The USGS currently operates and maintains two real-time lake water surface elevation gauges at the Saline (Gunnison Bay) and Saltair (Gilbert Bay) marinas (Figure 1). As described earlier, the causeway structure has created a water imbalance, which causes a higher lake water surface elevation in Gilbert Bay. Gauging station data show that the elevations of Gilbert Bay fluctuate between 0.06 to 0.2 meters higher than the elevation of Gunnison Bay, since the construction of the GSL Breach in 1984.

The closed lake basin of the GSL is sensitive to fluctuations in lake level as a

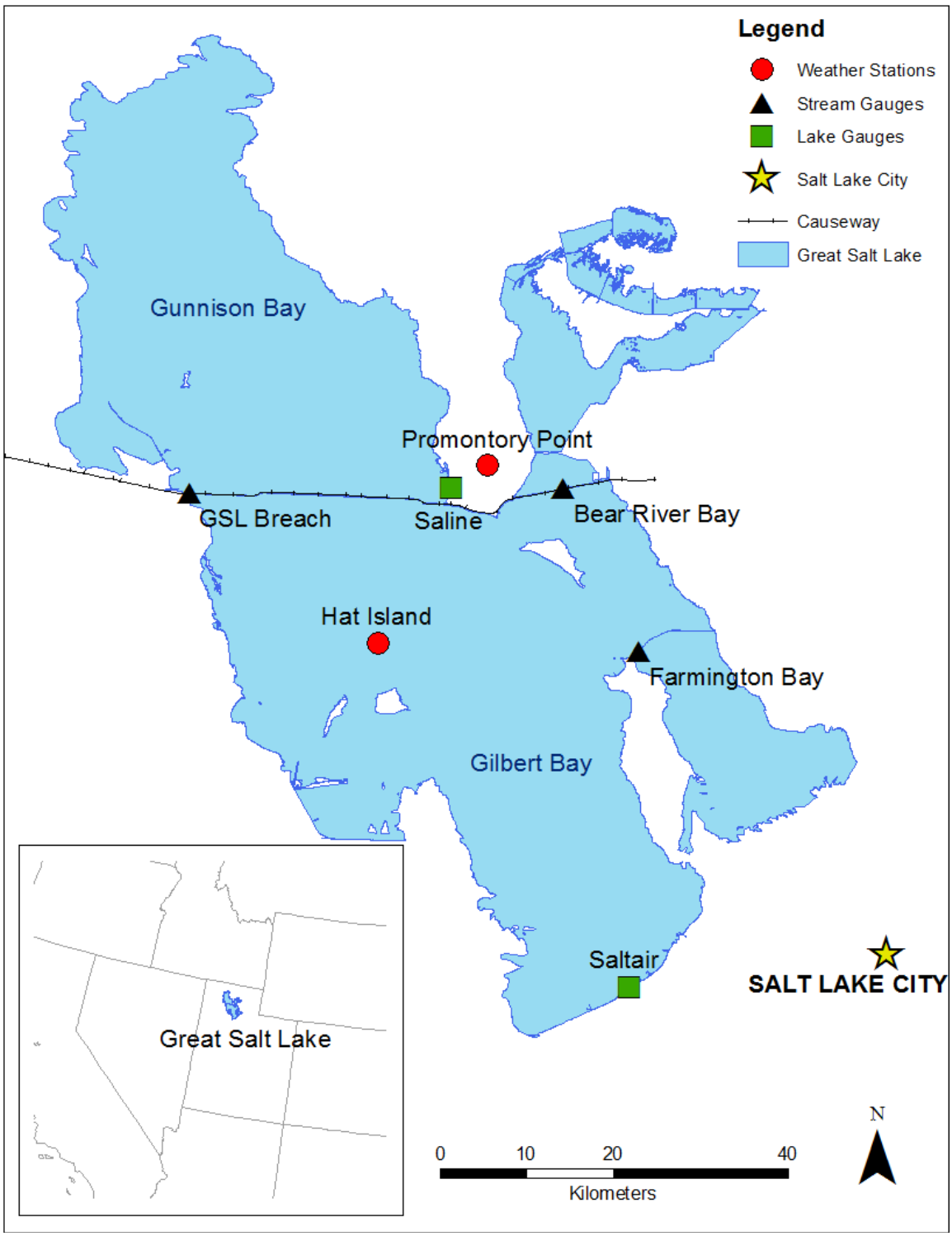

Figure 1. Location of Great Salt Lake causeway, causeway stream gauges, lake elevation gauges, and the Hat Island and Promontory Point weather stations, Great Salt Lake, Utah.

result of climatic and anthropogenic influences. In 1963, GSL reached its historic low water surface elevation at 1277.4 meters (Loving et al., 2000). In 1986, the lake reached its historic maximum water surface elevation at 1283.8 meters (Loving et al., 2000). The long-term elevation record of GSL (1847-present) indicates that lake fluctuations occur over time scales of 5 to 20 years or longer (Mohammed and Tarboton, 2012). Within the decadal patterns of lake elevation fluctuations, the lake has subannual fluctuations of approximately 0.5 m (1 to 2 feet). Over the course of a year, the lake level is affected by direct precipitation and input of snowmelt during the spring runoff season (March to June). The GSL level drops during the summer and fall (July to November) when evaporation is high and inflows are low, due to allotted divertment and irrigation. As the lake level changes, the volumes of the GSL subbasins fluctuate, resulting in concentration or dilution of the salts in the lake water.

Figure 2a shows the GSL water surface elevation from 1847 to 2013. Figure 2b shows the GSL water surface elevation observed during the 5-year study period (WY 2009-2013). Using the methods outlined in Mohammed and Tarboton (2012), the 25th, 50th, and 75th percentiles were computed for mean annual lake water surface elevations from 1847 to 2013 for Gilbert Bay. The annual lake water surface elevations for the 25th, 50^{th}, and 75th percentiles are 1279.3-m, 1280.3-m, and 1281.1-m, respectively. Considering the GSL history over the longer term, it is clear that conditions during our study period (WY 2009-2013) are not representative of average lake conditions, as lake water surface elevations are low, plotting below the 25th percentile during most of the study period (Figure 2b).

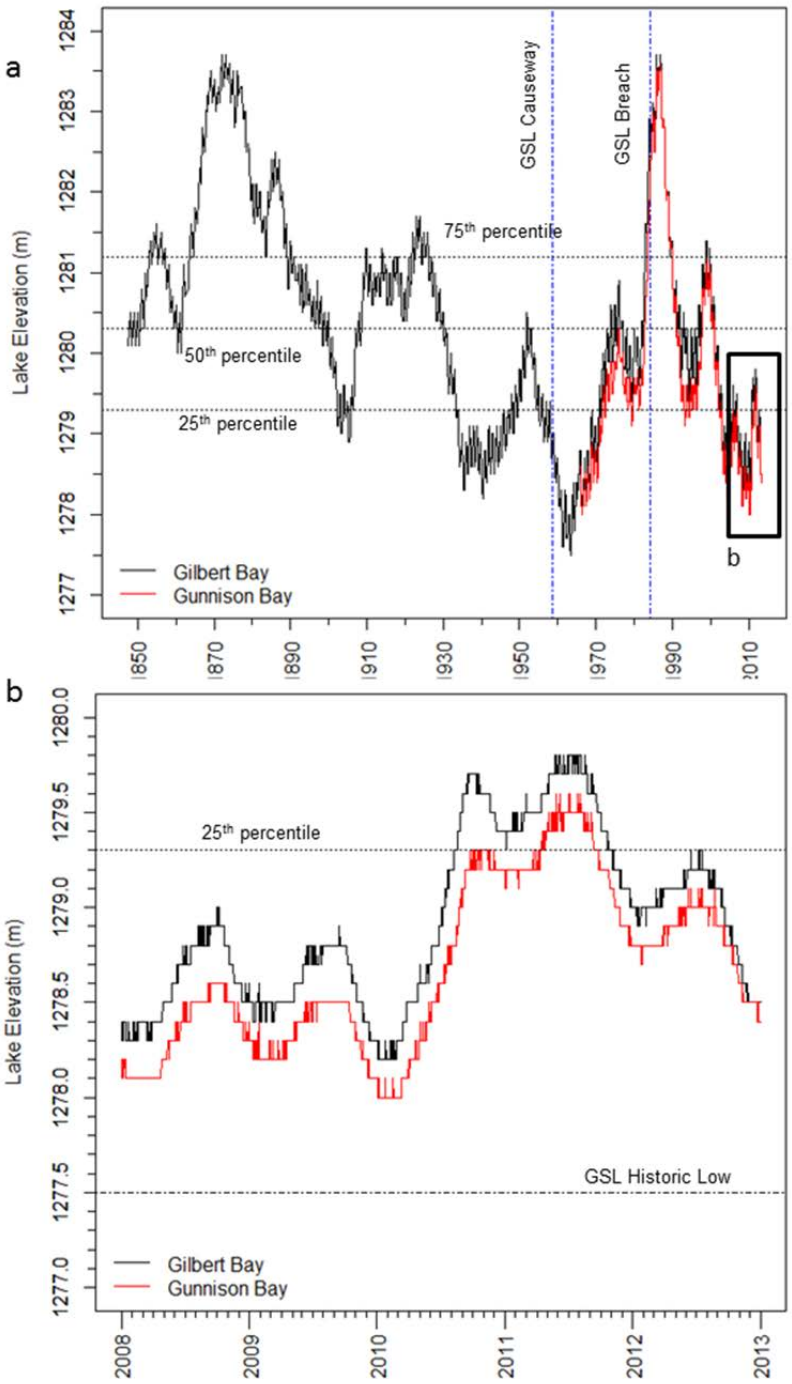

Figure 2. GSL lake elevation from (a) 1847 to 2013 with mean annual lake surface elevation percentiles (25th, 50th, and 75th percentiles) in meters (1279.3, 1280.3, and 1281.1, respectively) represented by the horizontal dashed lines and the construction of the GSL causeway and GSL Breach represented by the vertical dashed lines; (b) GSL lake elevation during the study period (WY 2009 to 2013) with the 25th percentile of mean lake elevation and the historic low stand of GSL represented by the horizontal dashed lines.

2.4 Great Salt Lake Hydrologic Flow Monitoring

Water transport across the GSL causeway has been monitored by frequent point measurements made by the USGS and the State of Utah since the causeway was first constructed in 1959 (Johnson and Loving, 2002; Loving et al., 2000). Recently, impacts of trace element and nutrient inputs to GSL has increased the need for monitoring the lake hydrodynamics to better resolve the variations in spatial and temporal distribution of water, salt, nutrients, and trace metals that affect chemical loading of GSL (Beisner et al., 2009; Carling et al., 2011; Diaz et al., 2009a; Diaz et al., 2009b; Dicataldo et al., 2011; Naftz et al., 2013; Naftz et al., 2008; Naftz et al., In Press; Naftz et al., 2011; Naftz et al., 2009; Oliver et al., 2009; Wurtsbaugh et al., 2011).

Growing concerns about impacts of anthropogenic activities on the lake have leveraged an increase of monitoring equipment across the basin. Over the last ten years, additional monitoring infrastructure has been added to the GSL. Three real-time stream gauging stations for surface water flows were installed at the railroad breach locations of Bear River Bay and GSL Breach, as well as the vehicle causeway breach of Farmington Bay. For the purpose of this study, data were analyzed from the GSL Breach, Saltair, and Saline hydrologic gauging stations (Table 1) (Figure 1).

Stream gauging instrumentation measures discharge at the GSL Breach gauging station in both the positive and negative directions. Positive discharge indicates flow from south-to-north (Gilbert Bay to Gunnison Bay), which is the prevailing flow direction at the GSL Breach. Negative discharge values indicate flow from north-to-south (Gunnison Bay to Gilbert Bay) across the causeway structure, which are uncommon occurrences at the gauging station. The negative discharge events recorded at

Table 1

Hydrologic and meteorological station information for predictor variables collected for GAM analysis. Hydrologic datasets are obtained from the USGS NWIS database and meteorological datasets obtained from the University of Utah MesoWest database.

Station Name	Site ID	Latitude (Decimal Degrees)	Longitude (Decimal Degrees)	Measured Variables	Period of records
Hydrological Data					
GSL Breach at Lakeside, UT	10010020	41.2225	112.8492	Stage (m), Discharge (m^3/s)	October 1, 2008 to September 30, 2013
Great Salt Lake at Saltair Boat Harbor, UT	10010000	40.7314	112.2128	Elevation (m)	October 1, 2008 to September 30, 2013
Great Salt Lake near Saline, UT	10010100	41.2553	112.4961	Elevation (m)	October 1, 2008 to September 30, 2013
Meteorological Data					
Hat Island	HATUT	41.0706	112.5851	Wind Direction (°), Sustained Wind Speed (m/s), Wind Gust (m/s)	October 1, 2008 to September 30, 2013
Promontory Point	PRP	41.2575	112.4398	Wind Direction (°), Sustained Wind Speed (m/s), Wind Gust (m/s)	October 1, 2008 to September 30, 2013

the GSL Breach are reversals (FRE) that transport hypersaline water from Gunnison Bay into Gilbert Bay (Naftz et al., In Press).

3. METHODOLOGY

3.1 Meteorological Datasets

Meteorological data for this study were collected at Hat Island and Promontory Point weather stations (Table 1) (Figure 1). Data were acquired from the University of Utah Department of Atmospheric Sciences MesoWest database over the time frame from October 1, 2008 to September 30, 2013 (University of Utah MesoWest, 2013). Meteorological parameters obtained from MesoWest include: 15-minute average wind direction, 15-minute maximum wind gust (m/s), and 15-minute sustained average wind speed (m/s)(Table 1). Data from the two weather stations contained several values that were considered erroneous and were not reported by MesoWest or they were recorded as a 'NULL' or 0.00 value. These erroneous values are a result of instrumentation error. All erroneous values reported within the meteorological data were omitted from the data used in this study.

3.2 Hydrological Data Collection

Lake water surface elevations are reported as elevation above NGVD27 (National Geodetic Vertical Datum of 1927). The operation and computation of lake elevation of Gunnison and Gilbert bays are recorded at the Saline (USGS Site ID: 10010100) and Saltair (USGS Site ID: 10010000) lake gauging stations. The lake gauging stations are operated and maintained by USGS following the methods outlined in Rantz and others

(1982a).

The GSL Breach (USGS Site ID: 10010020) measures and records stream stage and water velocity at 15-minute intervals. Stream stage measures the change in water surface height measured at the stream gauging station. Stream stage is set to an arbitrary elevation datum, unlike the lake gauging stations that report lake water surface elevation above NGVD27. The stage sensor is located on the south side of the GSL causeway and is an indirect measurement of lake water surface elevation of Gilbert Bay.

Water velocity is measured using a fixed-deployment SonTek Argonaut XR acoustic Doppler velocity meter (ADVM). The ADVM transmits an acoustic signal that is used to measure the velocity and direction of particles in the water using the Doppler principal. Fixed-deployment ADVMs are able to profile the water-column, determining current patterns and water stratification in bays, harbors, lakes, and rivers (U.S. Geological Survey, 2014). Water velocity readings are measured as both positive and negative values and used to compute discharge in a similar direction using index velocity methods (Levesque and Oberg, 2012). All hydrologic data collected at the GSL Breach are computed and published by USGS (Levesque and Oberg, 2012; Rantz and others, 1982b).

3.3 Hydrologic Datasets

Hydrologic data used during this analysis were obtained from the USGS National Water Information System (NWIS) database (http://waterdata.usgs.gov/nwis) over a 5-year period, WY 2009-2013 (October 1, 2008 to September 30, 2013) (Table 1) (U.S. Geological Survey, 2013a). Similar to meteorological data, several days contain missing

values when equipment malfunctioned at the various gauging stations. Erroneous data are reported as a 'NULL' or '0.00' value. These values were omitted from the data analyzed in this study. October 1, 2008 is the earliest date that real-time data were recorded at the GSL Breach. All hydrologic data were collected and recorded at 15-minute intervals. Hydrologic data in this study include GSL lake elevation (m) measured at Saltair Boat Harbor, UT and Saline, UT, stream stage (m), and discharge (m^3/s) from the GSL Breach at Lakeside, UT (Figure 1) (Table 1).

3.4 Palmer Drought Severity Index

Over the 5-year study interval (WY 2009-2013), Palmer Drought Severity Index (PDSI) (Palmer, 1965) values were retrieved from the National Oceanic and Atmospheric Administration (NOAA) National Climatic Data Center (NCDC) website (http://www.ncdc.noaa.gov/cdo-web/datasets) (National Climatic Data Center (NCDC), National Oceanic and Atmospheric Administration (NOAA), 2014). Drought severity data include index values from the state of Utah (State Code = 42) within the Northern Mountains division (Division = 05). The areal coverage of Division 05 includes the majority of the GSL drainage basin and tributaries that contribute freshwater input to the lake.

3.5 Flow Reversal Event Evaluation

A main goal of this research was to assess the characteristics of FREs, including the frequency and duration of their occurrence at the GSL Breach, which is the primary point of water and brine exchange between the partitioned bays of the GSL given the

recent closure of the GSL culverts. Fifteen-minute discharge data from the GSL Breach was used to identify FREs. To determine the temporal duration of a FRE, the beginning of an event was distinguished by the first negative value identified in the data. The next positive discharge value reported in the data indicated the end of the FRE. Each 15-minute negative discharge value was selected and the numbers of consecutive readings were summed for each event. The summed value was multiplied by 15-minutes to determine the total duration of the FRE. For example, if an event contained 10 consecutive negative discharge values, the duration of the FRE would be 150 minutes (10 readings x 15 minutes). The total number of FREs were compiled for the duration of the 5-year analysis period (WY 2009-2013) and further classified by individual water year (i.e., 2009, 2010, 2011, 2012, and 2013). Frequency and average duration of a FRE was further assessed for each month.

3.6 Generalized Additive Model

A GAM was used to evaluate the relative importance of the various hydrologic and meteorological variables that influence direction and magnitude of discharge across the GSL Breach over the 5-year study period. The computation of a GAM is described in equation 1:

$$y_i = \beta_0 + f_1(x_{1i}) + f_2(x_{ki}) + \cdots + \epsilon_i$$

where = y_i is a response variable for the ith observation, β_0 = a model matrix for parametric and suitably transformed predictor variables, f_k = are smooth functions for predictor variables, x_{ki} and ϵ_i are error terms that are independently and identically distributed random variables (Hastie and Tibshirani, 1990; Wood, 2006). GAMs were

performed in the statistical software R environment (R, 2013), using the *mgcv* package (Wood, 2014). All GAMs used a Gaussian (i.e., normal distribution) family. For these analyses, default arguments from the *gam* function in R were used with smoothing splines applied to all predictor variables defined in Table 2.

After the GAM models were developed, discharge was predicted based on the corresponding 15-minute hydrologic and meteorological predictor data. Following the computation of 15-minute discharge data, a mean daily discharge was computed for each day. Modeled daily discharge values were compared to USGS published daily values from the GSL Breach to verify model accuracy (U.S. Geological Survey, 2013a). Models were used to evaluate the influence of different variables and possible combinations of variables for predicting discharge

3.7 Cross-Validation of Generalized Additive Model

Cross-validation techniques were performed to test the GAM accuracy of predicting discharge at the GSL Breach. Cross-validation was performed using model GH10 as it was the best fitting model in this analysis (Table 2). Data from individual water years (2009, 2010, 2011, 2012, and 2013) were withheld from the dataset and the GAM model was run using the predictor variables for GH10. The five models that were generated were then used to compute discharge for each year that data were withheld from the GAM. Daily values were then computed and compared to observed daily values measured at the GSL Breach gauging station to determine prediction errors of the GAM.

Table 2

Model identification number, variables, and statistical summaries of GAMs. Model's identification are represented by the GAM model number and the contributing hydrologic and meteorological data used over the 5-year study period (water years 2009-2013): GGSL (GAM GSL), GH (GAM Hat Island), GP (GAM Promontory Point)). EDF (estimated degrees of freedom), Akaike information criterion (AIC), Generalized Cross Validation (GCV).

Model	Year Data Withheld	Variables	Model Coefficient									
			Intercept	Std Error	t-value	p-value	EDF	R^2 (adj)	Deviance Explained	GCV Score	AIC Score	n
GGSL1		Discharge ~ s(Saline) + s(Saltair)	26.8	0.052	517	<2e-16	19.0	0.571	57.1%	368	1200530	137248
GGSL2		Discharge ~ s(Saline) + s(Saltair) + s(Stage)	26.8	0.041	651	<2e-16	27.9	0.729	72.9%	232	1137531	137248
GH1		Discharge ~ s(Hat_Wind) + s(Hat_Dir)	26.8	0.076	354	<2e-16	18.1	0.082	8.2%	788	1304919	137248
GH2		Discharge ~ s(Hat_Gust) + s(Hat_Dir)	26.8	0.076	353	<2e-16	18.4	0.081	8.1%	789	1305045	137248
GH3		Discharge ~ s(Hat_Wind) + s(Hat_Dir) + s(Saline)	26.8	0.052	517	<2e-16	27.5	0.570	57.0%	369	1200717	137248
GH4		Discharge ~ s(Hat_Gust) + s(Hat_Dir) + s(Saline)	26.8	0.052	516	<2e-16	27.3	0.569	56.9%	369	1200980	137248
GH5		Discharge ~ s(Hat_Wind) + s(Hat_Dir) + s(Saltair)	26.8	0.051	527	<2e-16	27.6	0.587	58.7%	354	1195203	137248
GH6		Discharge ~ s(Hat_Gust) + s(Hat_Dir) + s(Saltair)	26.8	0.051	526	<2e-16	27.5	0.586	58.6%	356	1195678	137248
GH7		Discharge ~ s(Hat_Wind) + s(Hat_Dir) + s(Saline) + s(Saltair)	26.8	0.046	580	<2e-16	36.8	0.659	65.9%	293	1168891	137248
GH8		Discharge ~ s(Hat_Gust) + s(Hat_Dir) + s(Saline) + s(Saltair)	26.8	0.046	580	<2e-16	36.3	0.659	65.9%	293	1169019	137248
GH9		Discharge ~ s(Hat_Wind) + s(Hat_Dir) + s(Saline) + s(Saltair) + s(stage)	26.8	0.039	689	<2e-16	45.8	0.758	75.8%	208	1121977	137248
GH10		Discharge ~ s(Hat_Gust) + s(Hat_Dir) + s(Saline) + s(Saltair) + s(stage)	26.8	0.039	689	<2e-16	45.8	0.758	75.8%	208	1121745	137248
GP1		Discharge ~ s(Prom_Wind) + s(Prom_Dir)	26.8	0.077	347	<2e-16	17.8	0.049	4.9%	817	1309788	137248
GP2		Discharge ~ s(Prom_Gust) + s(Prom_Dir)	26.8	0.077	347	<2e-16	18.0	0.046	4.6%	819	1310193	137248
GP3		Discharge ~ s(Prom_Wind) + s(Prom_Dir) + s(Saline)	26.8	0.054	500	<2e-16	27.6	0.541	54.1%	395	1209910	137248
GP4		Discharge ~ s(Prom_Gust) + s(Prom_Dir) + s(Saline)	26.8	0.054	499	<2e-16	25.5	0.539	53.9%	396	1210490	137248
GP5		Discharge ~ s(Prom_Wind) + s(Prom_Dir) + s(Saltair)	26.8	0.053	509	<2e-16	27.4	0.557	55.7%	380	1204862	137248
GP6		Discharge ~ s(Prom_Gust) + s(Prom_Dir) + s(Saltair)	26.8	0.053	507	<2e-16	27.3	0.554	55.4%	383	1205745	137248
GP7		Discharge ~ s(Prom_Wind) + s(Prom_Dir) + s(Saline) + s(Saltair)	26.8	0.048	560	<2e-16	36.6	0.634	63.4%	314	1178786	137248
GP8		Discharge ~ s(Prom_Gust) + s(Prom_Dir) + s(Saline) + s(Saltair)	26.8	0.048	558	<2e-16	35.3	0.632	63.2%	316	1179574	137248
GP9		Discharge ~ s(Prom_Wind) + s(Prom_Dir) + s(Saline) + s(Saltair) + s(stage)	26.8	0.040	678	<2e-16	45.6	0.750	75.0%	215	1126392	137248
GP10		Discharge ~ s(Prom_Gust) + s(Prom_Dir) + s(Saline) + s(Saltair) + s(stage)	26.8	0.039	679	<2e-16	45.2	0.751	75.1%	214	1125911	137248

4. RESULTS AND DISCUSSION

4.1 Flow Reversal Events Summary

Fifteen-minute discharge values measured at the GSL Breach ranged from -166 m^3/s to 340 m^3/s over the analysis period (WY 2009-2013) (U.S. Geological Survey, 2013a). In comparison, the Colorado River near Cisco, UT has an average discharge of approximately 225 m^3/s during the month of April (U.S. Geological Survey, 2013a). Table 3 summarizes attributes of the FREs observed and recorded at the GSL Breach gauging station. During the 5-year analysis period, a total of 1510 FREs were recorded at the GSL Breach gauging station, with an average of 302 events occurring each year. Several FREs were short in duration, lasting 15-minutes or less, with consideration that shorter duration events cannot be identified because the rate of data collection is limited to 15-minutes. The longest event recorded at the GSL Breach was 1950-minutes (32.5 hours), recorded on April 7-9, 2013 (Figure 3). Over the 5-year period, the average duration of a FRE lasted approximately 96 minutes, with the median time of 30 minutes. The 2009 WY recorded the most FREs, amounting to 414 occurrences in total: however, the average duration of an event was shorter in comparison with other years, with an average duration of 57.1 minutes. FREs recorded during the 2012 WY had the longest average duration per event, 141 minutes.

Figure 4 shows that FREs occur more frequently in September through December, with November and October having the highest number of events per month. The greater

Table 3
Summary of FREs recorded at the GSL Breach gauging station from October 1, 2008 to September 30, 2013 (WY 2009-2013).

	Total (2009 to 20013)	WY 2009	WY 2010	WY 2011	WY 2012	WY 2013
Total Number of Events	1510	414	159	396	248	293
Event per day	0.83	1.13	0.44	1.08	0.68	0.8
Average Duration (minutes)	95.5	57.1	132.5	58.6	141.2	140.8
Median Duration (minutes)	30	30	45	30	60	60
Minimum Events (minutes)	15	15	15	15	15	15
Maximum Event (minutes)	1950	840	1920	915	1650	1950
Average number of events per year	302					

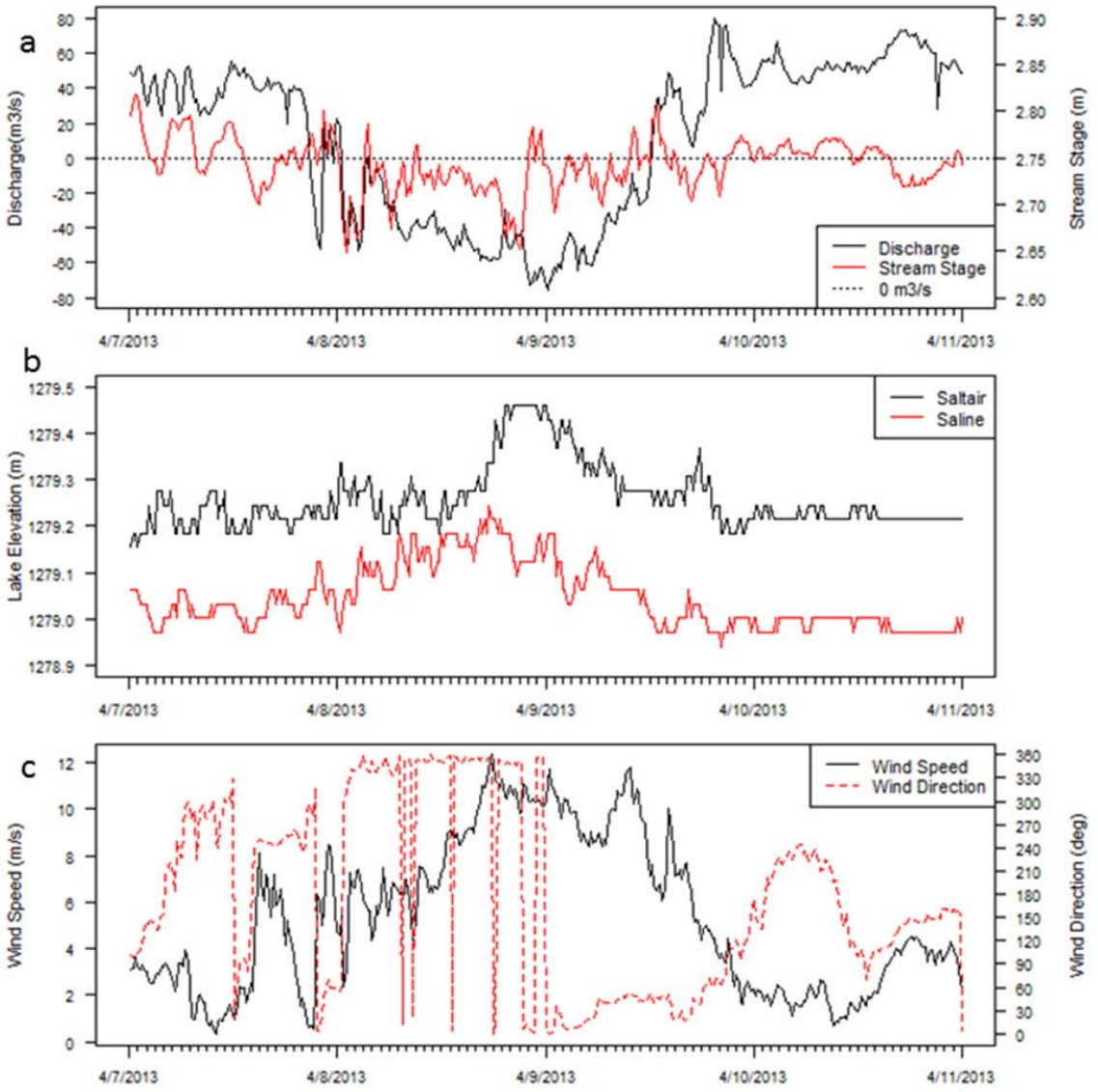

Figure 3. Time-series analysis of a FRE occurring on April 8 - 9, 2013. Time-series data includes: a) discharge and stream stage measured at the GSL Breach stream gauging station, b) lake water surface elevation measured at Saltair and Saline lake gauges, and c) wind speed and wind direction measured at Hat Island weather station. The FRE lasted approximately 1950 minutes (32.5 hours) and is the largest FRE recorded at the GSL Breach in the study interval WY 2009-2013.

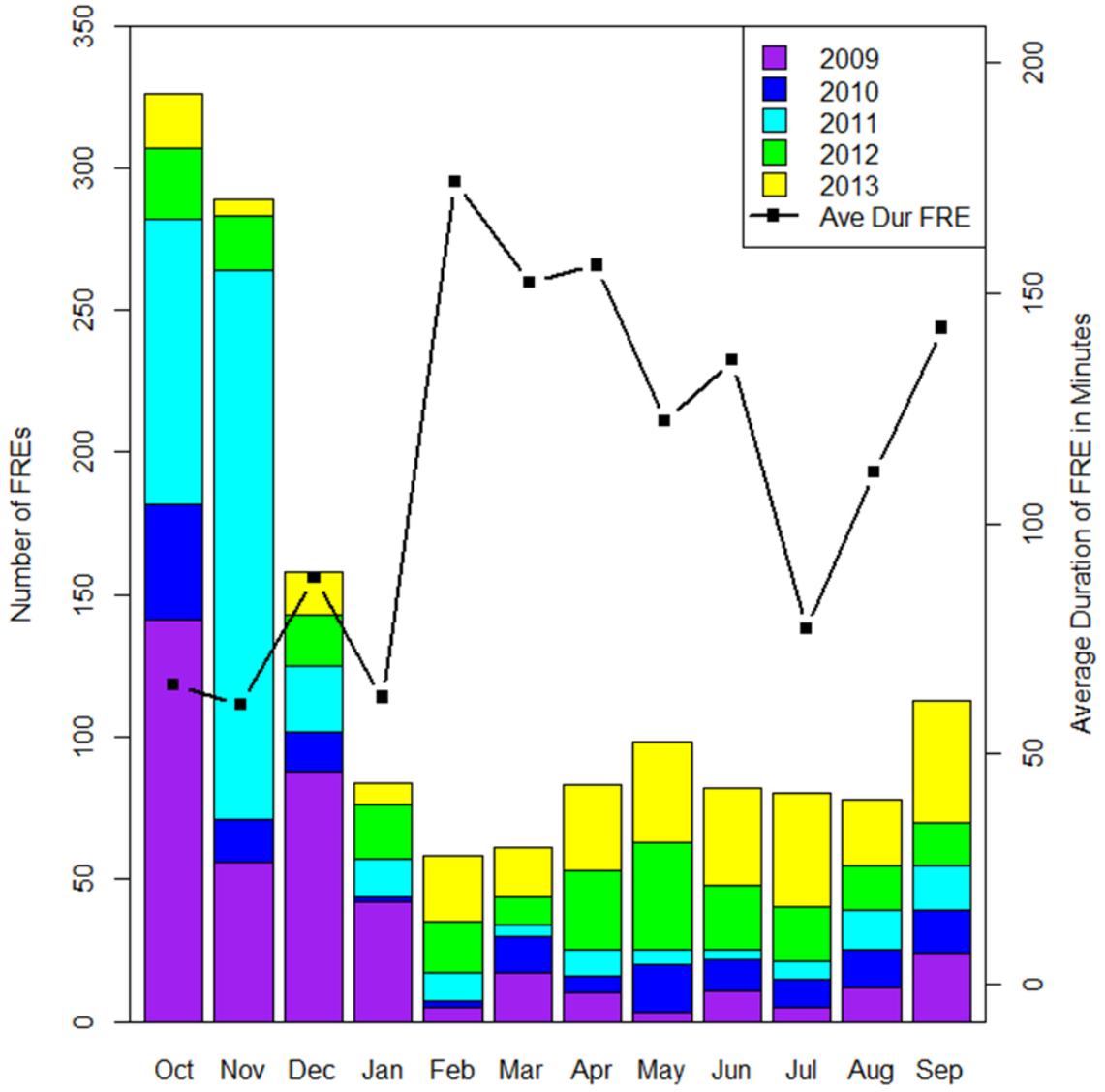

Figure 4. Flow Reversal Events at the GSL Breach gauging station recorded during the study interval (WY 2009-2013) with bar plots representing the number of FREs occurring each month. The line plot represents the average duration of a FRE in minutes for each month observed during the study period.

frequency of FRE during the late summer and fall months are attributed to declining inflow volumes due to irrigation diversions upstream of the GSL and increased evaporation. These conditions reduce the differences in lake water surface elevation between Gilbert and Gunnison bays, thus reducing hydrologic head gradient to approximately 0.06 m, or lower as observed in 2013 (Figure 2b). The summer and fall seasonal influences and diversions increase the frequency of FREs observed during those months.

Over the study period, FREs were less frequent during the months of January through August. During the winter months (January through February), evaporation is low and diversions of GSL influent tributaries are minimal, resulting in increased discharge into GSL. Beginning in February and March, melting snow within the lower elevations of the watershed increases the volume of freshwater inflows to GSL. The increase in discharge causes the water surface elevation of Gilbert Bay to increase at a more rapid rate as compared to the water surface elevation of Gunnison Bay. The water surface elevation in Gunnison Bay increases at a slower rate as a result of the railroad causeway, where inflow to the north arm is restricted to the GSL Breach.

The difference in lake water surface elevations between Gilbert and Gunnison bays continue to increase from April through June during the runoff season. These conditions are easily identified when looking at a hydrograph of the 2009 WY (Figure 5). The largest difference in water surface elevation is observed in June, when Gilbert Bay has a water surface elevation that is approximately 0.2 m or higher than the water surface elevation of Gunnison Bay. The 0.2+ meter hydrologic head difference between the two bays causes the flow direction at the causeway to be primarily from Gilbert Bay to

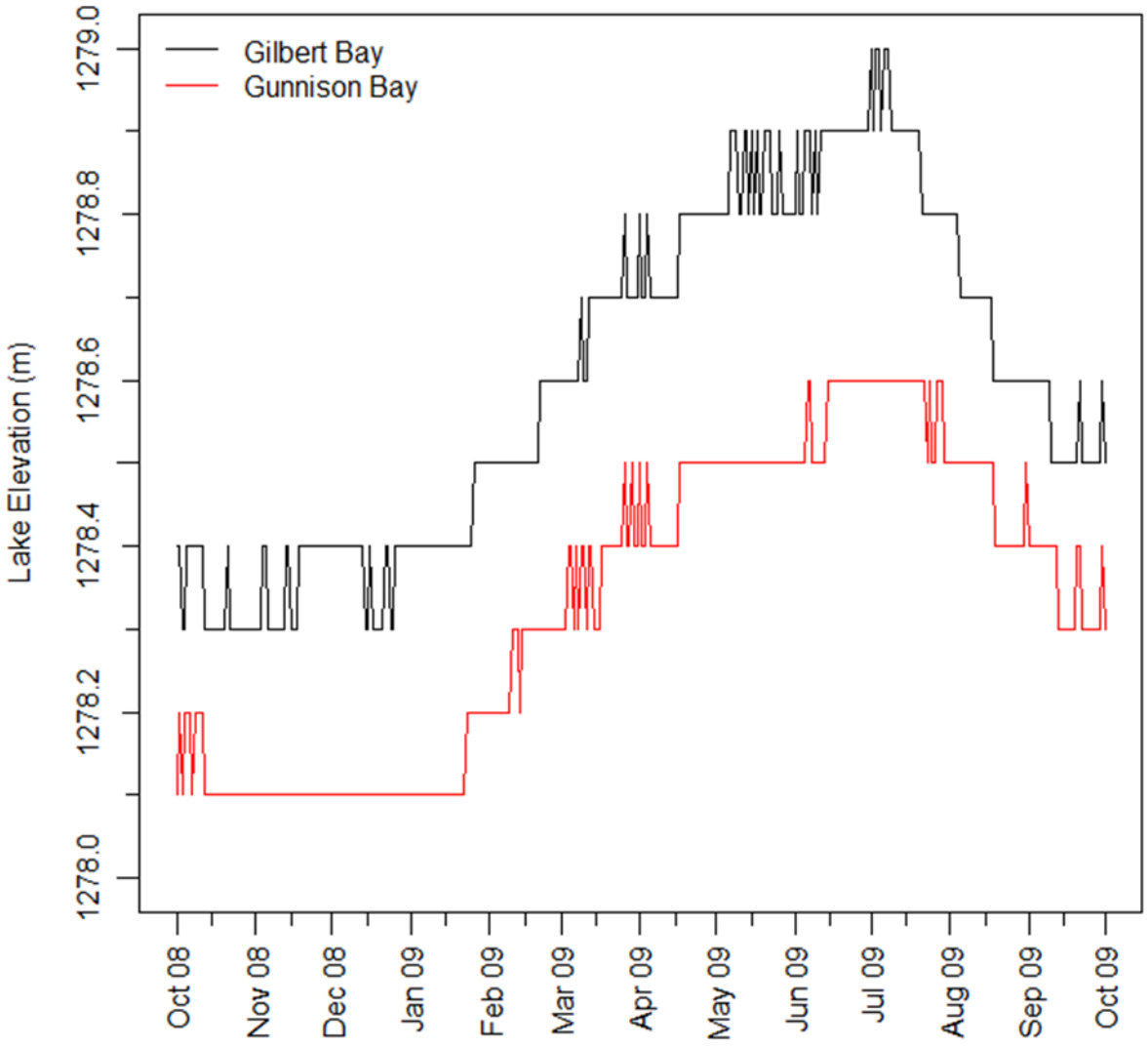

Figure 5. Mean daily lake water surface elevations measured at the Saltair and Saline Lake gauging stations showing the fluctuations in water surface elevations and the differences observed between Gilbert and Gunnison bays over the 2009 WY.

Gunnison Bay (south-to-north). The lower frequency of FREs observed from January to August suggests that the greater difference in lake water surface elevations (> 0.1 m) between Gilbert and Gunnison bays reduces the number of FREs at the GSL Breach.

In addition to the frequency of FREs, we determined the average duration of these events. FREs that occurred during October through January were more frequent, but the average duration of an event typically lasted less than an hour (Figure 4). In contrast, the months of February, March, and April had the fewest number of FREs, but events lasted for several hours (Figure 4). During these months, the average FRE lasted approximately 140 minutes, with events in February having the longest average duration at 174 minutes.

The FREs observed during these spring months appear to have a similar response to the timing and duration of lake-effect precipitation events that impact the urban areas east of the GSL. GSL lake-effect precipitation events are observed during the cool-season (September 16 to May 15), with the primary maximum events occurring during October and November and a secondary maximum occurring in March and April (Alcott et al., 2012; Alcott and Steenburgh, 2013; Yeager et al., 2013). During March and April, the passage of large synoptic systems through the Great Basin region is correlated with dust storm events (Hahnenberger and Nicoll, 2012; Hahnenberger and Nicoll, 2014). Dust storms result from strong prefrontal southerly winds, followed by a transition to strong northerly winds after the passing of the cold front. Northern winds preceding the passage of cold fronts are hypothesized to be a driving force of FRE at the GSL Breach.

4.2 Case Study of Flow Reversal Event: April 27-28, 2010

To evaluate the conditions at the GSL Breach during a FRE, we assessed a storm event on April 27-28, 2010 (Figure 6). Beginning on April 27, 2010, a storm system passed across the GSL basin, resulting in strong (wind speeds >10 m/s) prefrontal winds from a southwesterly direction (~ 210 degrees). As shown in Figure 6, when the southwesterly winds began to increase in magnitude, the lake water surface elevations of both Saltair and Saline began to decrease in elevation. As lake water surface elevation decreased at the lake gauging stations, discharge at the GSL Breach began to increase from 25 m^3/s to a peak of 42.5 m^3/s at 18:30 hours on April 27, 2010. This peak in discharge at the GSL Breach coincides with lower lake water surface elevation recorded at the Saline lake gauge (Prior event = 1278.5 m, during event = 1278.3 m). This suggests that the water within Gunnison Bay was displaced to the northern reaches of the bay, reducing the water surface elevation by approximately -0.2 m on the northern side of the GSL causeway. In comparison, the water of Gilbert Bay was also displaced by the southwesterly winds, resulting in decreased lake water surface elevation measured at the Saltair lake gauge (Prior event = 1278.8 m, during event = 1278.6 m). As the water of Gilbert Bay was displaced to the north along the GSL causeway, the hydrologic head gradient increased. Figure 7 provides a schematic of how a southerly wind displaces water within the GSL basin affecting hydrologic head at the GSL causeway.

The increase in the lake water surface elevation along the southern side of the GSL causeway is observed in the stream stage measurements at the GSL Breach gauging station. Stream stage recorded at the GSL Breach is an indirect measurement of the lake water surface elevation recorded at the GSL Breach. Prior to the increase in

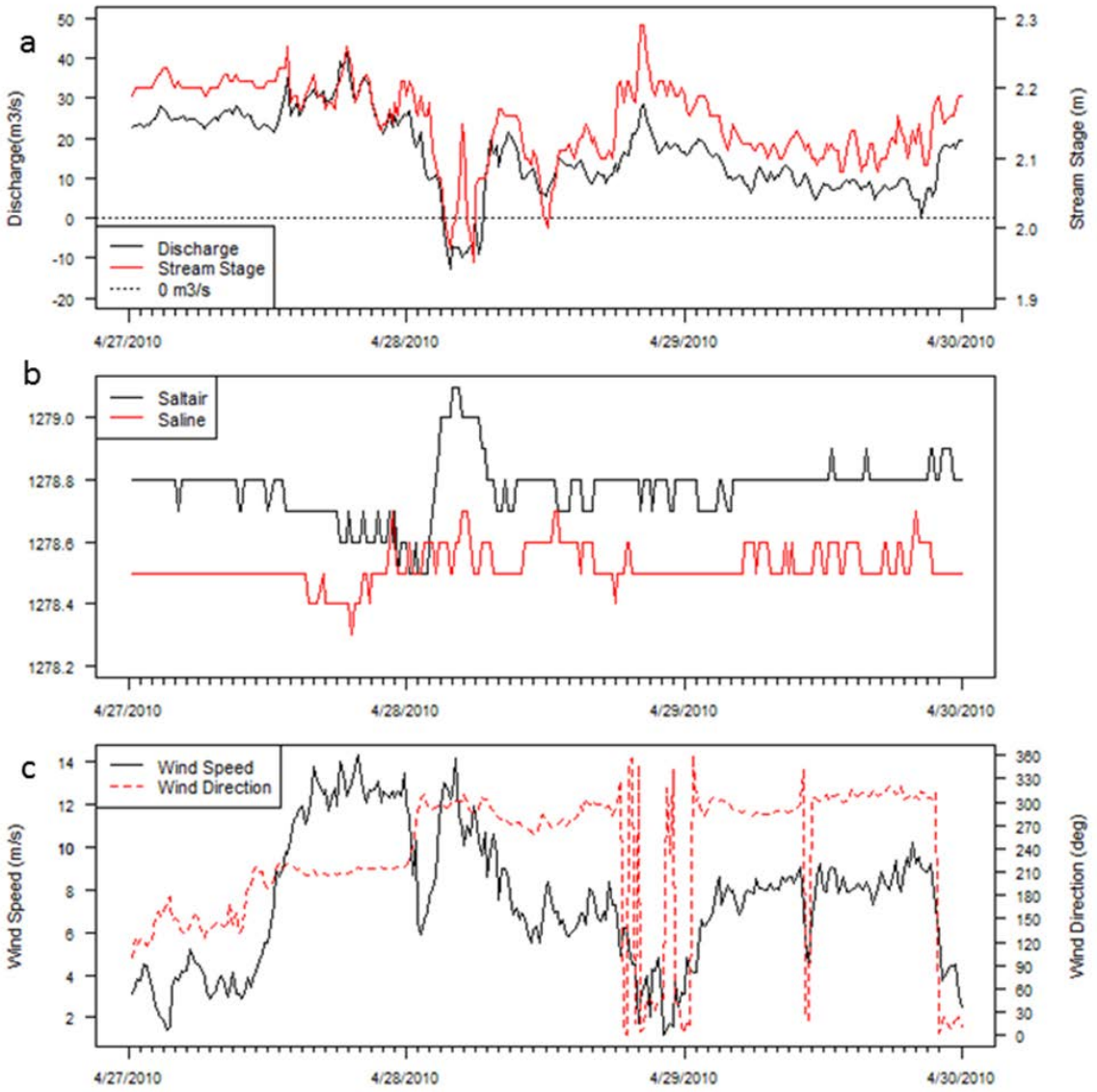

Figure 6. Time-series analysis of the FRE on April 27-28, 2010. Figures include time-series plots of a) discharge and stream stage measured at the GSL Breach stream gauging station, b) lake water surface elevation measured at Saltair and Saline lake gauges, and c) wind speed and wind direction measured at Hat Island weather station.

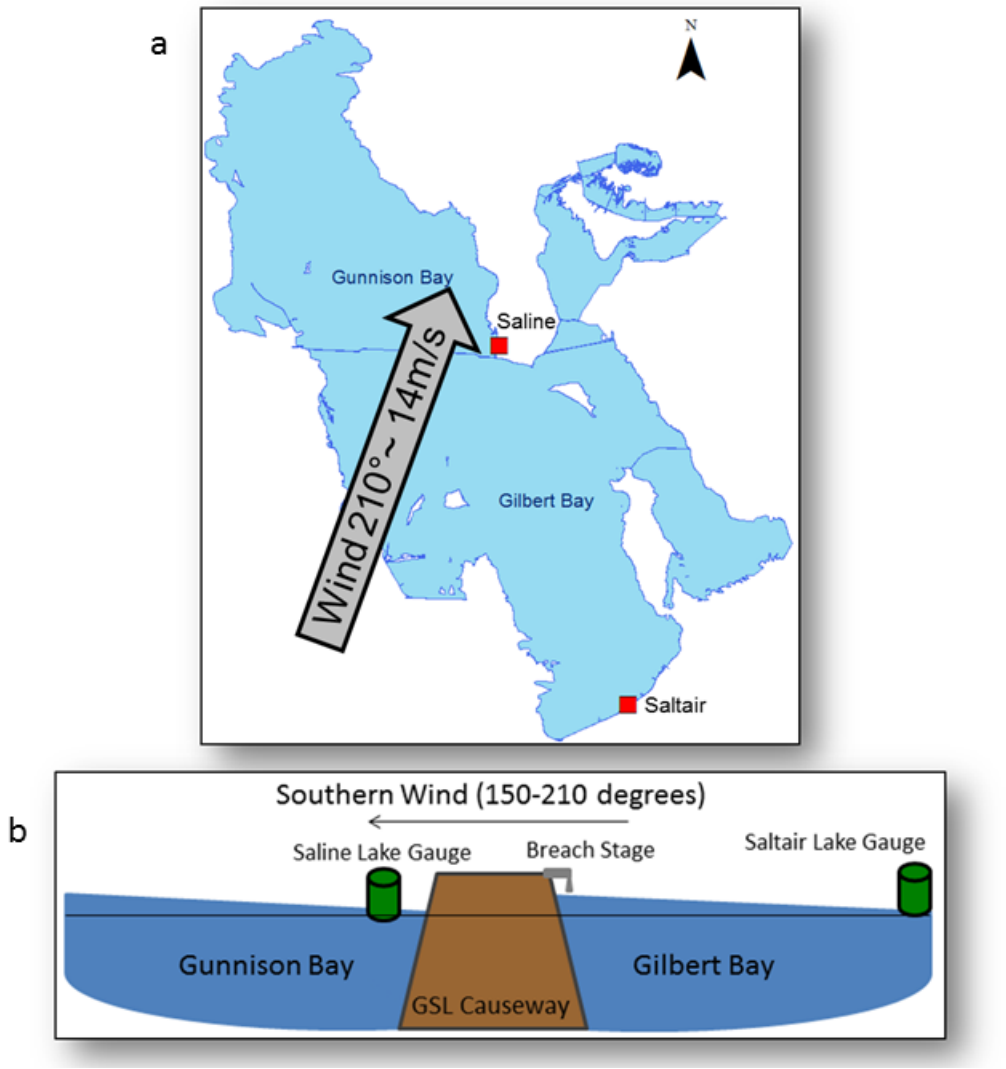

Figure 7. Schematic showing how a) a southern wind blowing across the GSL b) displaces water to the northern extents within Gilbert and Gunnison bays. As water is displaced, the hydrologic head gradient observed at the GSL causeway changes with respect to wind direction, influencing flow direction and magnitude of discharge at the GSL Breach. A strong south wind results in an increase in positive discharge values measured at the GSL Breach.

southwesterly winds on April 27, stream stage at the GSL Breach was approximately 2.20 m. During the southern wind event, stream stage peaked at 2.26 m, coinciding withthe peak discharge event at 18:30 hours on April 27, 2010. This is a 0.06 m increase in hydrologic head observed at the GSL Breach, verifying that southerly wind events displace water to the north along the GSL causeway within Gilbert Bay.

Around 01:00 hours on April 28, 2010, the front had passed over the GSL basin, and winds shifted from a southwest direction to a northwest direction (320-330 degrees) and maintained wind speeds of greater than 10 m/s for approximately three hours (Figure 6). When the wind direction shifted to the northwest, water was displaced to the southern boundaries of Gilbert and Gunnison bays, which resulted in an increase in lake water surface elevation measured at both the Saltair and Saline lake gauges. Saltair measured the largest change in lake water surface elevation with a 0.5 m change (Positive peak = 1278.6 m, Negative peak = 1279.1 m) between the positive peak discharge to the negative peak of the FRE. The Saline lake gauge recorded a smaller change in water surface elevation with 0.4 m (Positive Peak = 1278.3 m, Negative peak = 1278.7 m). As the northern wind displaces the water to the southern boundaries of each bay, both lake gauges record an increase in lake water surface elevation (Figure 6) (Figure 8). When both lake gauges show the increase in lake water surface elevation, discharge at the GSL Breach was recorded as a negative discharge event representing a FRE. As water is 'pushed' south by the northwesterly winds, the water surface elevation decreased along the southern side of the GSL causeway.

Stream stage verified the change in hydrologic head as water was pushed south of the GSL causeway within Gilbert Bay. During the FRE, stream stage dropped from 2.26

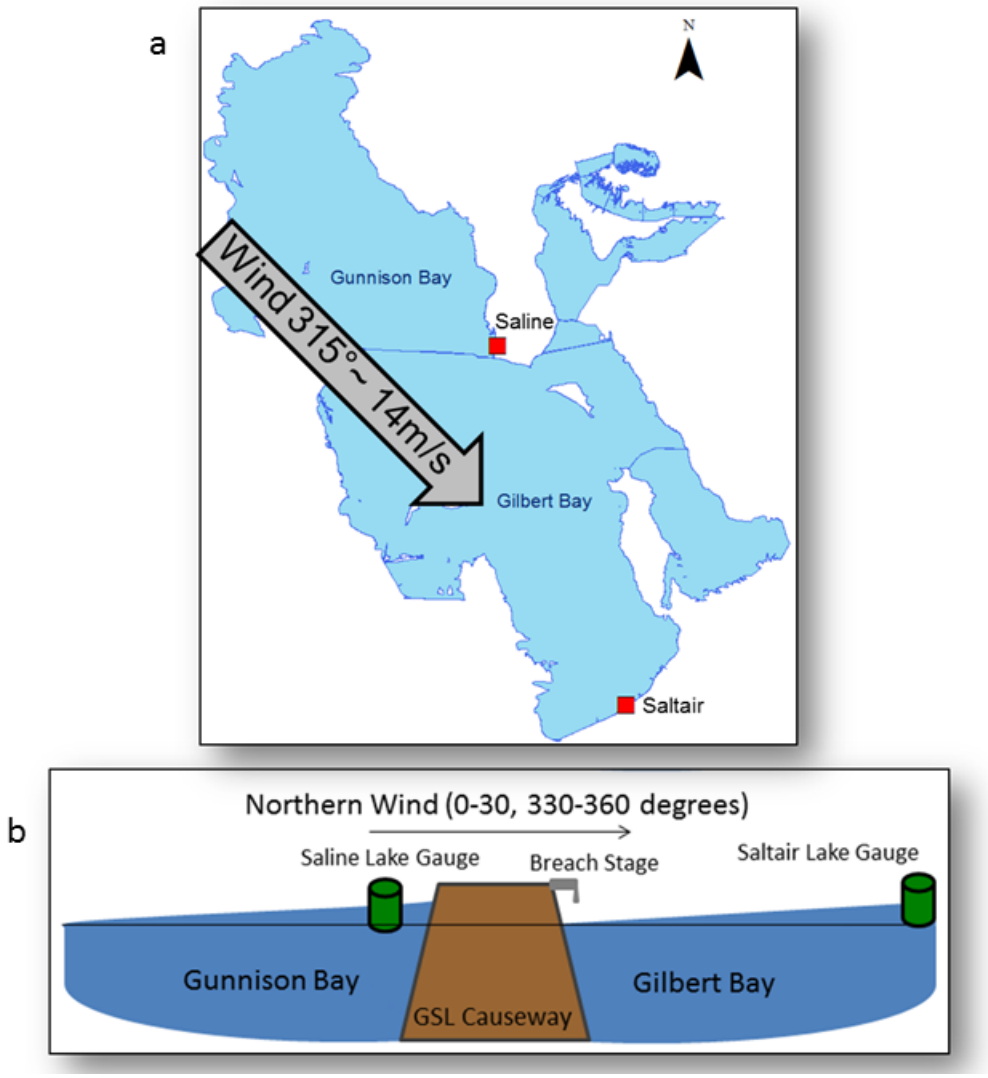

Figure 8. Schematic showing how a) a northern wind blowing across the GSL b) displaces water to the southern extents within Gilbert and Gunnison bays. As water is displaced, the hydrologic head gradient observed at the GSL causeway changes with respect to wind direction, influencing flow direction and magnitude of discharge at the GSL Breach. A strong sustained northerly wind results in FRE (north-to-south flow) at the GSL Breach.

m to 1.95 m, resulting in a -0.31 m change in lake water surface elevation measured at the GSL Breach. The change in stream stage at the gauging station suggests a change in thehydrologic head gradient between Gunnison and Gilbert Bay. The stream stage sensor is located on the south side of the GSL causeway bridge; therefore, the stream stage readings reflect the lake water surface elevations of Gilbert Bay. However, it is assumed that when the stream stage drops as a result of northerly wind events, the lake water surface elevation of Gunnison Bay is higher than the lake water surface elevation of Gilbert Bay, resulting in a FRE.

The results presented in this case study provide a basic example of hydrodynamics of the GSL. Quickly changing weather conditions are reflected in the hydrologic data which respond quickly to changing weather conditions. These observations suggest a minimal lag between storms crossing the GSL Basin and the response of the GSL.

4.3 Generalized Additive Model

4.3.1 Generalized Additive Model Development

During this study, multiple variations of hydrologic and meteorological variables were used to predict discharge at the GSL Breach using the GAM method. A total of 22 models were developed for this study (Table 2). Two models (GGSL1-2) were developed using only hydrologic predictor variables. Model GGSL1 uses only lake elevation at Saltair and Saline gauging stations whereas model GGSL2 uses lake elevation and stage data collected from the GSL Breach gauging station as predictor variables. Models GH1, GH2, GP1, and GP2 used meteorological predictor variables

from Hat Island (GH1-2) and Promontory Point (GP1-2) and no hydrologic predictor variables during model development. Additional models were developed using both hydrologic and meteorological variables. The models were divided into two scenarios based on the meteorological station used in each GAM; one scenario used Hat Island (GH3 through GH10) and the other modeled scenario used Promontory Point (GP3 through GP10) weather station data with additive hydrological variables to each GAM.

Statistical summaries of each GAM (Table 2), including standard error, GCV score, AIC, and deviance explained by individual terms (R^2), were used to identify the ideal combination of predictor variables for modeling discharge at the GSL Breach. Individual models were used to explore combination of variables and their explanatory power. Sample size for all GAM were 137,248 with p-values of < 2e-16 for all models.

Models GGSL1and GGSL2 used only hydrological predictor variables to predict discharge at the GSL Breach. GGSL1, which only uses lake elevation from Saline and Saltair lake elevation gauging station as predictor variables, resulted in an R^2 of 0.571 with a GCV score of 368. Model GGSL2, which includes stage data collected at the GSL Breach stream gauging station, resulted in an R^2 value 0.729 and a GCV score of 232. GAMs that used only meteorological predictor variables (GH1-2 and GP1-2) had low R^2 values that range from 0.046 to 0.082 and had high GCV scores ranging from 819 to 788, thus suggesting that wind alone is insufficient for modeling discharge at the GSL Breach. A comparison of the models that used meteorological and hydrological data individually suggests that the lake water surface elevations of Gilbert and Gunnison bays influence discharge at the GSL Breach more than meteorological variables. The addition of stage data within the GAM resulted in significant improvement in model accuracy, thus

confirming that stage can be used as an indicator of lake elevation at the GSL Breach improving model accuracy.

Previous research has explained the influences of wind affecting GSL hydrodynamic properties, including lake seiches or wind tides (Lin, 1977), lake circulation (Rich, 2002; Spall, 2009), vertical mixing (Beisner et al., 2009), and flooding (Atwood, 2002). More recently, Naftz (In press) explained that sustained winds from a northerly direction result in FREs across the GSL Breach, transporting hypersaline waters of Gunnison Bay into Gilbert Bay. The relationship between wind and lake elevation was investigated in additional modeling scenarios using the GAM method.

Meteorological and hydrological variables were routinely added in various combinations for models GH3 through GH6 and GP3 through GP6. These models explored the relationship between meteorological predictor variables (wind direction, wind speed, and wind gust) with lake water surface elevations from either Saline or Saltair but not both stations at once. Models GH3 through GH6 had higher R^2 values (0.569 to 0.587) and lower GCV (369 to 354) and AIC scores (1200980 to 1195203) when compared to the Promontory Point models. GAMs using Hat Island weather data in combination with Saltair hydrological data had slightly higher R^2 values and lower AIC and GCV scores than models using Saline data. This suggests that the lake water surface elevations of Gilbert Bay are a significant influence on the discharge conditions observed at the GSL Breach.

The next set of models used meteorological data as well as both Saltair and Saline lake water surface elevation data as predictor variables (GH7, GH8, GP7, and GP8). Models that used Hat Island weather station data provided more accurate prediction of

discharge at the GSL Breach than GAMs that applied Promontory Point weather station data. R^2 values of 0.659 were reported for models GH7 and GH8 and R^2 values of 0.634 and 0.632 were reported for GP7 and GP8, respectively. For models GH7 and GH8, there appears to be no difference between the model results when using 15-minute sustained wind speed data compared to 15-minute maximum wind gust data, as both models had similar R-square (0.659) and GCV scores (293). However, GH7 had a slightly lower AIC score compared to GH8, suggesting that sustained wind speed may serve as a better predictor variable for discharge at the GSL Breach. For GAMs using Promontory Point data, GP7, which uses 15-minute sustained wind speed data, is a better predictor variable than 15-minute wind gust data, having a higher R^2 value of 0.632 and lower GCV (314) and AIC (1178786) scores.

Stream stage was the final predictor variable applied to the GAM. As previously explained, stream stage, at the GSL Breach, provides an indirect measurement of lake water surface elevation, thus giving a more accurate measure of the lake water surface elevation at the stream gauging station. For models using Hat Island meteorological data, both models (GH9 and GH10) had R^2 values of 0.758 and GCV scores of 208. Model GH10 had a slightly lower AIC score of 1121745 when compared to GH9 (1121977), suggesting a slightly better fitting model when using wind gust as a predictor variable. For GAMs using Promontory Point meteorological data, GP10 had a slightly higher R^2 value (0.751), lower GCV (214) and AIC (1125911) scores when compared to GP9 (0.751, 215, and 1126392), suggesting that wind gusts, in combination with other meteorological and hydrological variables, provide a better predictor variable for the Promontory Point models.

Of the 22 models produced in this study, GAMs using wind gust as a predictor variable, in combination with wind direction, water surface lake elevation from Saltair and Saline, and stream stage from the GSL Breach, provide the best fitting models for both meteorological datasets (Hat Island and Promontory Point). Statistical summaries of the models produced in this study suggest that models using Promontory Point data were less significant than models developed using predictor variables from Hat Island weather data. This is most likely a result to the proximity of the Hat Island weather station to the GSL Breach. In addition, Hat Island weather station is located at a lower elevation (1293 m), which is within 14 m of the lake water surface elevation of GSL. This weather station is located at a central point in Gilbert Bay, approximately 28 km southeast of the GSL Breach (Figure 1). In contrast, the weather station for Promontory Point is located at an elevation of 2,111 meters in the Promontory Mountain range. The elevation of the weather station is approximately 830 m above the lake water surface elevation of GSL and the location is approximately 35 km east of the GSL Breach (Figure 1). The close proximity to the GSL Breach and lower elevation of the Hat Island weather station more accurately represents the weather conditions on the GSL, in contrast to Promontory Point weather station. The statistical results for GAMs using different weather data reflects the various microclimates operating within the GSL basin.

4.3.2 Generalized Additive Model Prediction

To further investigate the accuracy of the GAM and individual predictor variables used to determine discharge at the GSL Breach, published USGS daily discharge values at the GSL Breach were compared to the daily discharge values computed using models

GH7 through GH10 and GP7 through GP10. Residual plots of modeled and observed values were used to determine biases over the range of discharge observed during the 5-year study period at the GSL Breach. Model prediction errors were assessed by the root mean square error (RMSE) for each model.

Residual plots for mean daily discharge using GH7 and GH8 showed a low bias in the modeled values when compared to published mean daily discharge values from the GSL Breach (Figure 9). Models GH7 and GH8 showed a low bias for discharge values below 0.0 m^3/s and when discharge began to exceed 50 m^3/s. Outliers were observed throughout the range of observed and modeled discharges values, but were common when discharge exceeded 50 m^3/s. Outliers are discharge events that occur during storm events in both the positive and negative direction. Residual plots suggested a strong correlation of daily discharge values between 0 to 50 m^3/s. Reported RMSE values from the residual plots for GH7 and GH8 were 9.876 and 9.861, respectively.

Models using GH9 and GH10 indicated less of a bias when compared to models GH7 and GH8; however, modeled discharge values are still biased low for discharge values greater than 70 m^3/s and for discharge values less than 0 m^3/s. Similar to residual plots using GH7 and GH8, outliers exist throughout the range of discharge values but are more common when discharges exceed 50 m^3/s and when discharge drops below 0 m^3/s representing large storm events. RMSE values improved slightly with GH9 and GH10, reporting RMSE values of 8.728 and 8.691, respectively.

Residual plots using Promontory Point models GP7 through GP10 (Figure 10) show similar trends to the Hat Island models. Both GP7 and GP8 showed similar low biases for discharge values less than 0 m^3/s and for values greater than 50 m^3/s. Residual

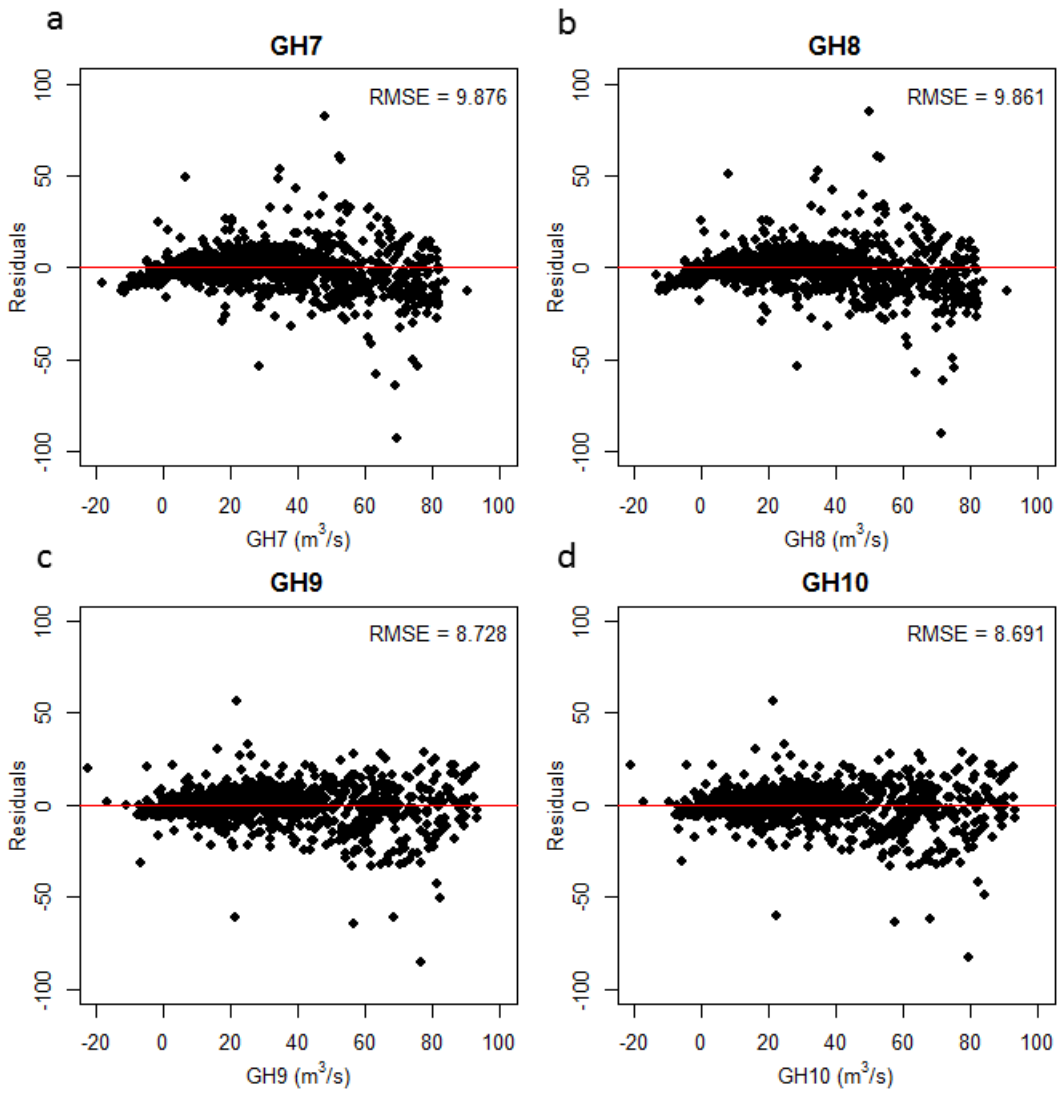

Figure 9. Residual plots with corresponding root mean square error (RMSE) values of modeled mean daily discharge and observed discharge at the GSL Breach, Great Salt Lake, Utah over the period of record in this study (WY 2009-2013). Residual plots include analysis using a) GH7, b) GH8, c) GH9, and d) GH10.

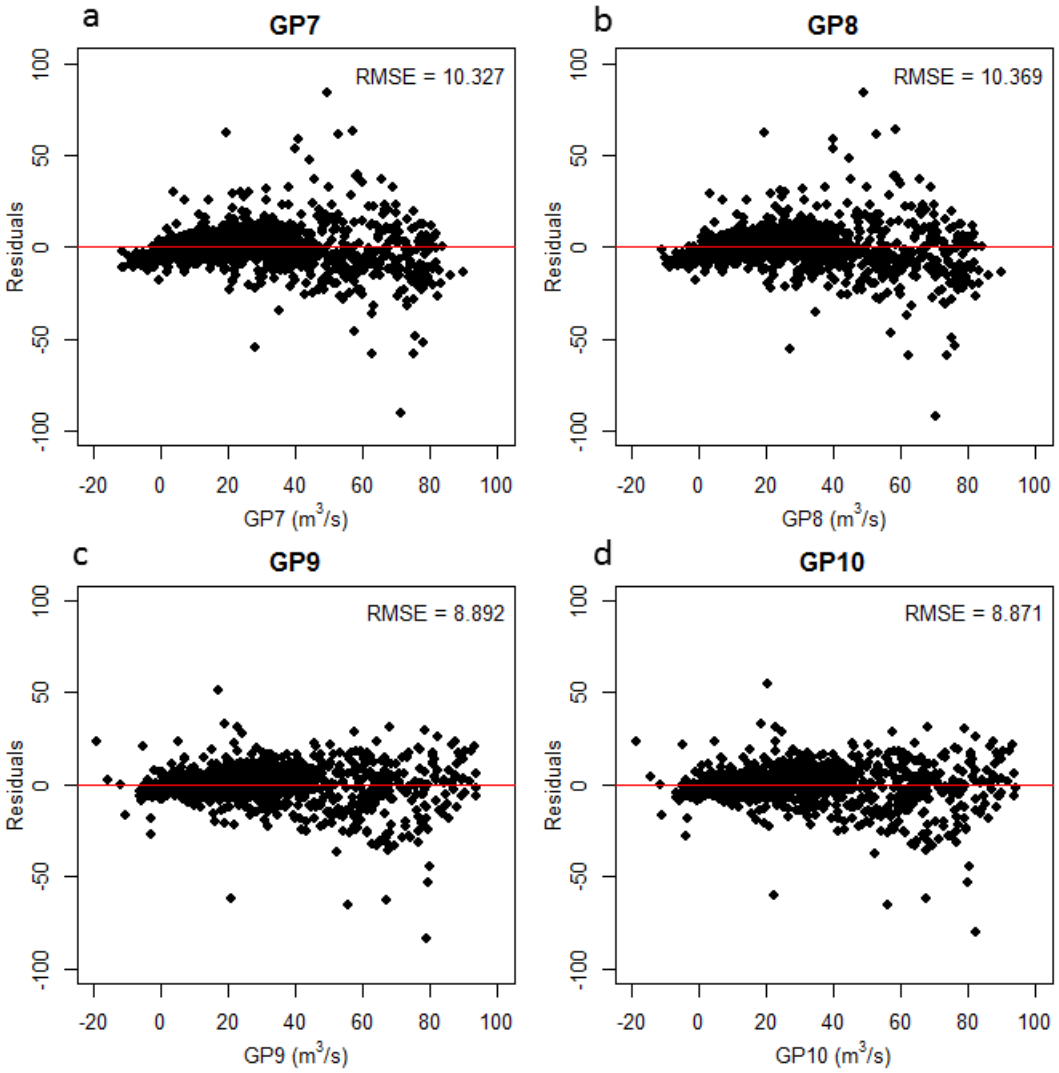

Figure 10. Residual plots with corresponding root mean square error (RMSE) values of modeled mean daily discharge and observed discharge at the GSL Breach, Great Salt Lake, Utah over the period of record in this study (WY 2009-2013). Residual plots include analysis using a) GP7, b) GP8, c) GP9, and d) GP10.

scatter plots of GP7 and GP8 show more variance in the range of measurements observed when compared to models GH7 and GH8 (Figure 9). This is represented in the higher RMSE values for models GP7 and GP8 having RMSE values of 10.327 and 10.369, respectively. These values are slightly higher than the RMSE values reported for the Hat Island residual plots.

Similar to GH9 and GH10, models using GP9 and GP10 indicated less bias when compared to models GP7 and GP8; however, modeled discharge values are biased low for discharge values greater than 70 m^3/s for discharge values less than 0 m^3/s, similar to residual plots from Hat Island. Promontory Point models GP9 and GP10 had RMSE values that were slightly higher than those reported for Hat Island, with GP9 and GP10 reporting RMSE values of 8.892 and 8.871, respectively.

The biases observed in the regression scatter plots were noticeable in time-series comparisons of mean daily discharge values. In Figures 11 and 12, observed and modeled discharge values are compared over a 3-month period (March 1, 2013 to June 1, 2013). In Figure 11, discharge values from models GH7, GH8, GP7, and GP8 consistently predicted discharge values less than the values published by USGS for numerous small discharge peaks in the positive flow direction. Time-series analysis corroborates low bias described in the residual plots for models GH7, GH8, GP7, and GP8 (Figures 9, 10). During FREs, discharge values from models GH7, GH8, GP7, and GP8 predict a positive discharge value when flows observed at the GSL Breach are reported as negative. This represents the low bias observed in the residual plots when discharge values at the GSL Breach are less than 0 m^3/s.

In Figure 11, the discharge values from models GH9, GH10, GP9, and GP10

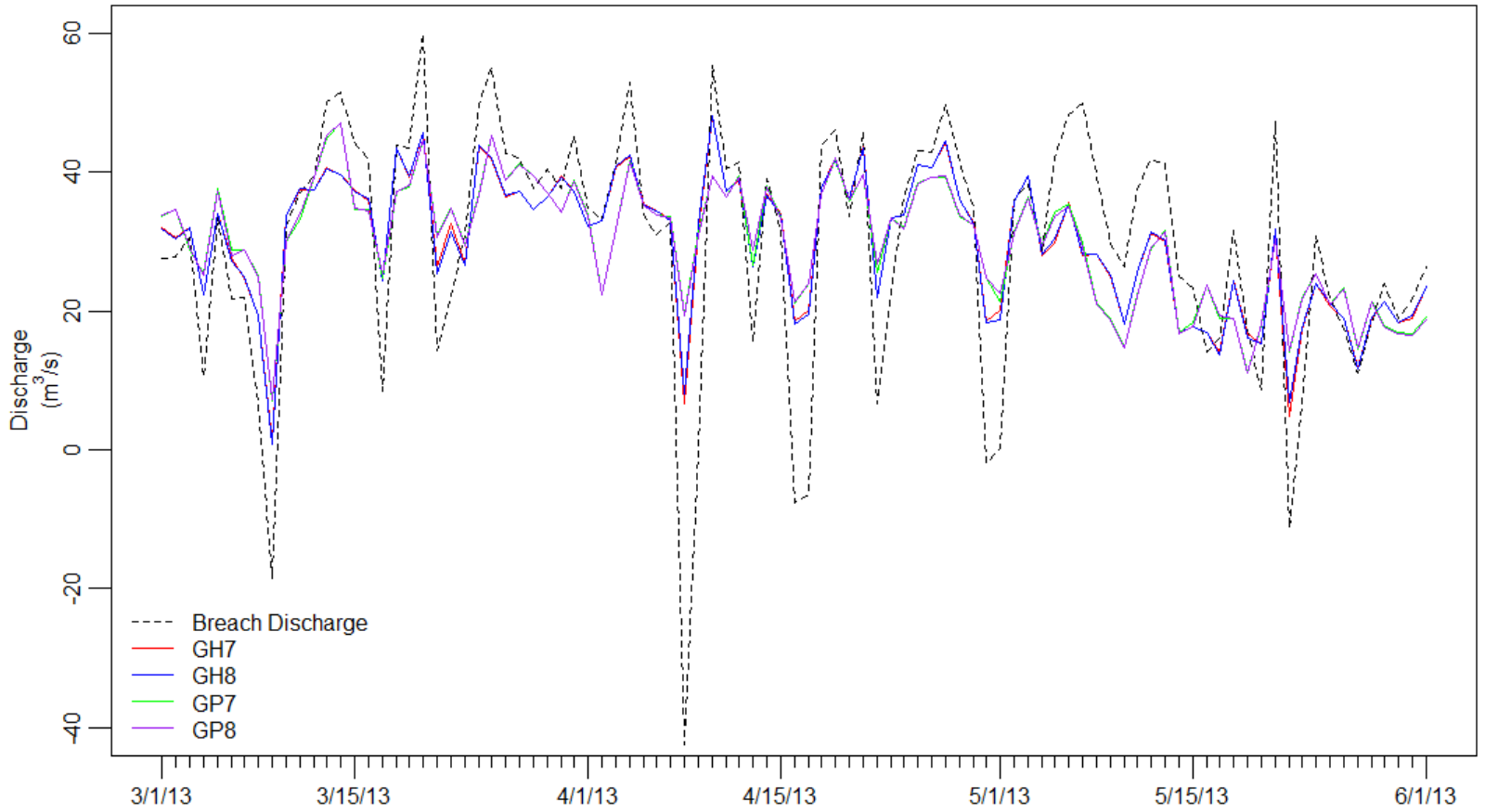

Figure 11. Time-series analysis of mean daily discharge values observed at the GSL Breach and predicted values using models GP7, GP8, GP7, and GP8. Comparisons show that modeled values are biased low during positive and negative peaks at the GSL Breach.

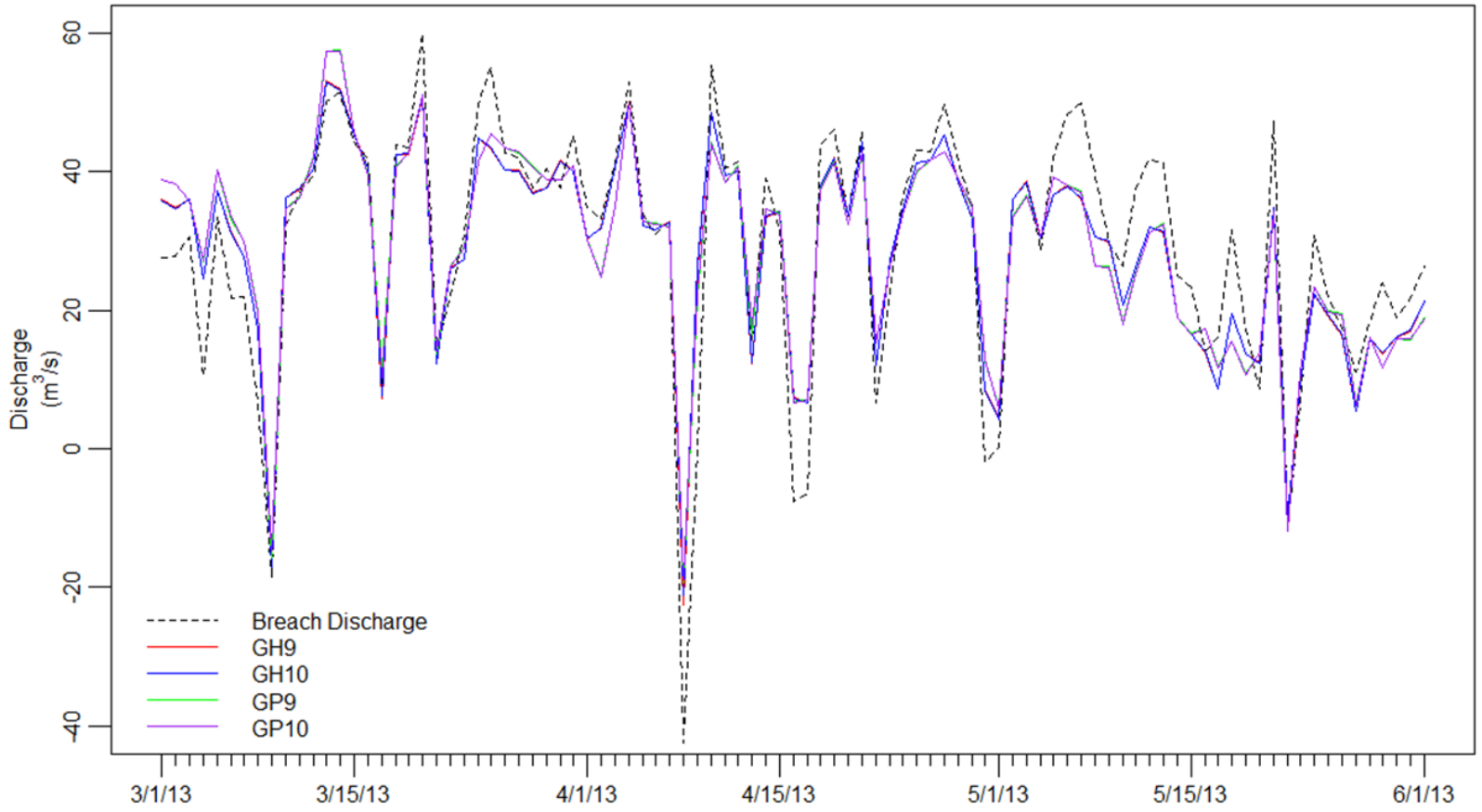

Figure 12. Time-series analysis of mean daily discharge values observed at the GSL Breach and predicted values using models GP9, GP10, GP9, and GP10. Comparisons show that modeled values are biased low during positive and negative peaks at the GSL Breach; however, model accuracy is greatly improved when using GP7, GP8, GP7, and GP8.

compare well with the discharge values measured and reported by USGS. Positive discharge peaks are accurately represented by the models, with a slight low bias in the results for some of the peaks observed in May. The FRE events recorded at the GSL Breach are also accurately predicted by models GH9, GH10, GP9, and GP10 both in magnitude and timing. The predicted negative discharge peaks on March 4, April 8, 16, 30 report smaller peaks than the observed peaks at the GSL Breach. This demonstrates the low bias described by the residual plots in Figures 8 and 9.

The mean daily discharge values observed at the GSL Breach gauging station ranged from 162 to -42.5 m^3/s over the 5-year study period. Mean daily discharge values predicted by models GH9 (93.2 to -22.5 m^3/s), GH10 (93.2 to -21.2 m^3/s), GP9 (93.8 to -19.3 m^3/s), and GP10 (94.0 to -19.0 m^3/s) were less than those measured and reported by USGS. The low bias observed in the residual plots for discharge values below 0 m^3/s is verified by the negative mean daily discharge values reported for models GH9, GH10, GP9, and GP10. The positive mean daily discharge values for the models are considerably less than the values reported by USGS. In addition to the low bias identified in the residual plots, modeled discharge values during storm events reported less discharge when compared to observed values. Peak discharge events during storm events are identified as outliers in the residual plots. Due to the dynamic conditions that occur during these events, it is difficult to accurately measure and model these discharge peaks.

Beginning in 2002, prolonged drought conditions persisted across the GSL drainage basin, and from 2009 to 2012, the lake water surface elevation of the GSL approached a historic low < 1279 m above sea level (Skorko et al., 2012). Comparing the GSL lake water surface elevations with the PDSI values related to regional precipitation

and air temperature, it is clear that drought conditions were prominent in the GSL basin prior to October 2010 (Figure 13). Beginning in November 2010, the PDSI values become positive, indicating cooler air temperatures and increased precipitation in the GSL basin (Figure 13). During the 2011 water year, all major tributaries to the GSL were above the 95 percent exceedance probability (U.S. Geological Survey, 2013b), resulting in one of the wettest intervals in recorded history, as reflected in the PDSI values for the GSL drainage basin (Figure 13). The abnormally wet conditions during 2011 resulted in a high volume of freshwater input to the GSL, and lake elevation rose nearly 1.7 meters within a nine-month period (Figure 13). The increased inflow to GSL raised discharge values recorded at the GSL Breach from 1 m^3/s observed in October 2010, to sustained flows of 100 m^3/s or greater, with a peak daily discharge of 159 m^3/s occurring on Jun 22, 2011 at the GSL Breach.

During the 2011 water year, missing hydrologic and meteorological data from May 18 to October 3 prevented calibration of the GAMs used in this study. The abrupt changes observed during the spring of 2011 in the lake water surface elevation records provided contrasting conditions to the lower lake levels and discharge volumes observed in WY 2009, 2010, 2012, and 2013. It is unfortunate that predictor variable data from the various hydrologic and meteorological datasets were not available during the wet period in 2011. If data were available for model calibration, it is suggested that the model accuracy for discharge values greater than 50 m^3/s would improve with the additional calibration points observed over the May 18, 2011 to October 3, 2011 time period.

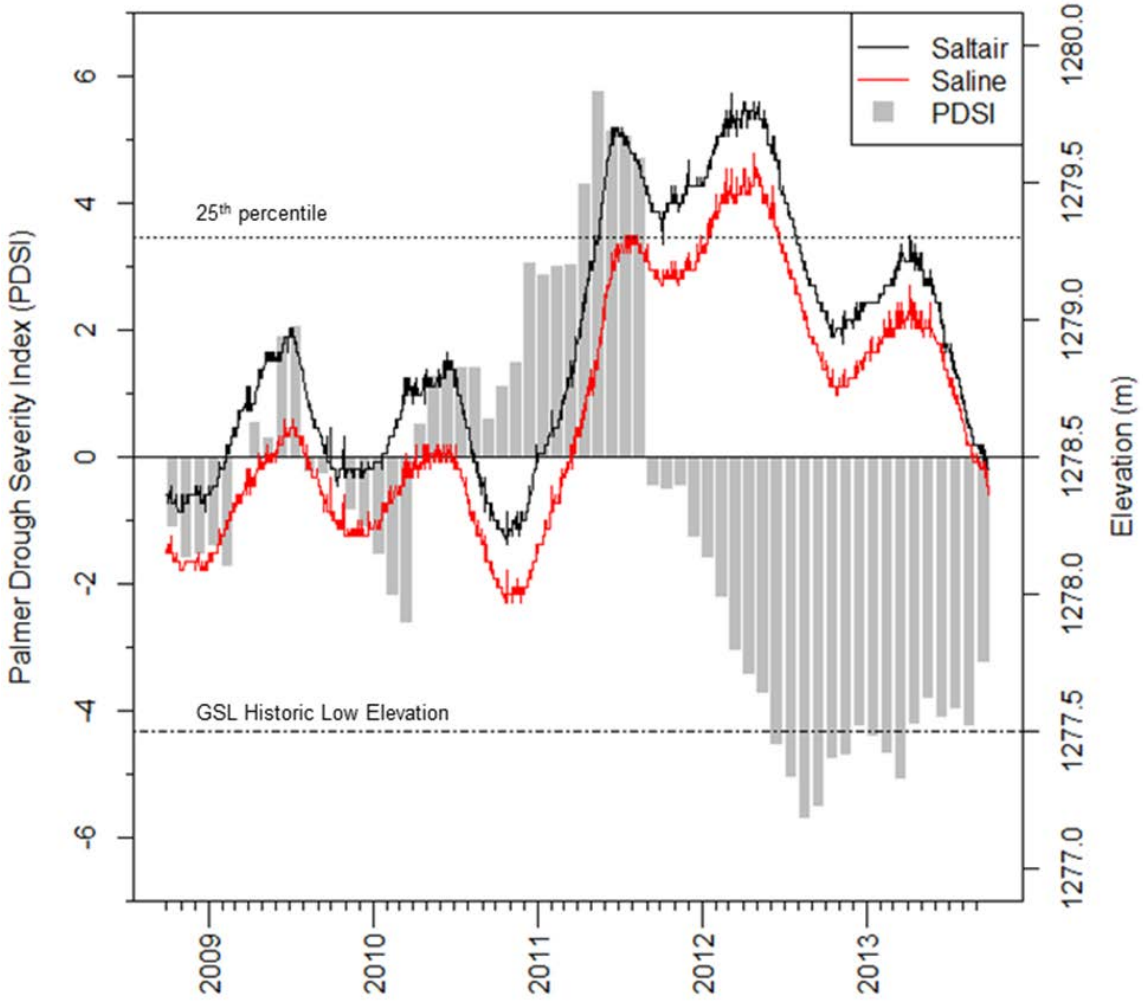

Figure 13. Lake elevation of Gilbert and Gunnison Bay from October 1, 2008 to September 30, 2013, with monthly Palmer Drought Severity Index (PDSI) for the GSL Drainage Basin. Dashed lines show the GSL historic low elevation and the 25th mean annual percentile.

4.3.3 Cross-Validation

Cross-validation techniques were performed to test the GAM validation of predicting discharge at the GSL Breach. Cross-validation was performed using model GH10 as it was the best fitting model in this analysis. Figure 14 shows the residual plots of observed discharge values at the GSL Breach and the predicted discharge values when withholding observed values from each water year. Figure 14 suggests that the predictive nature of the GAM performs well from 0 m^3/s to approximately 30 m^3/s. Discharge values less than 0 m^3/s show a low bias in the computed discharge values. As observed in Figures 9 and 10, models GH7-8 and GP7-8 were also biased low from discharge values that were less than 0 m^3/s. GH10 was biased low for discharge values that exceeded 60 m^3/s (Figure 9). However, cross-validation discharge predictions are biased high for discharge values that exceed 60 m^3/s. Residual plots in Figure 14 show additional scatter in the residuals, thus resulting in a higher RMSE value (41.69) when compared to the RMSE values presented in Figures 9 and 10. The increased range of scatter in the residuals observed above 30 m^3/s suggest that the GAM accuracy decreases once flows exceed 30 m^3/s and a high range of uncertainty is present when discharge values exceed 60 m^3/s due to limited calibration data as described earlier.

4.4 Generalized Additive Model Interpretation

4.4.1 Smoothed Term Plots

Smoothed term plots show the result of each linear term applied to the GAM. Smoothed term plots provide visual observations of the individual predictor variables applied to a GAM. Model GH10 was used to demonstrate the smoothed term predictions

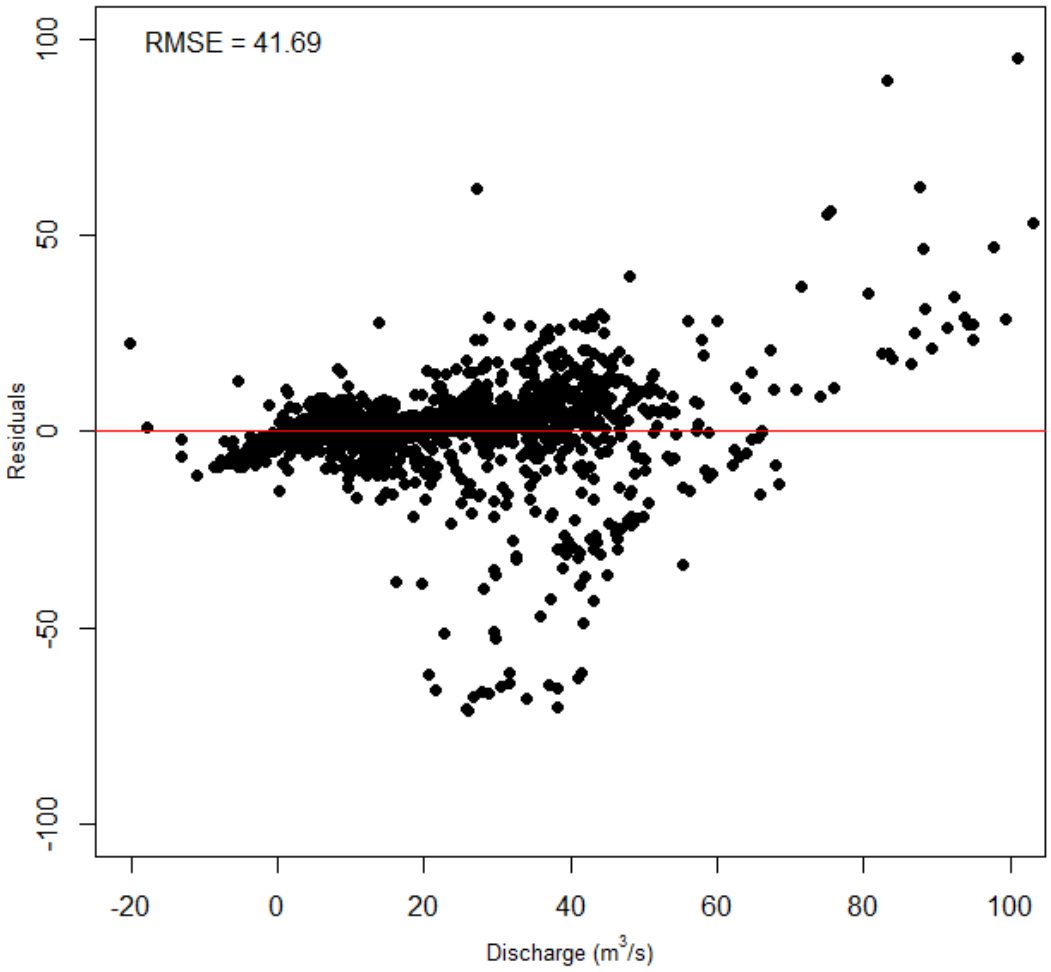

Figure 14. Cross-validation residual plots with corresponding root mean square error (RMSE) values of modeled mean daily discharge values and observed mean daily discharge at the GSL Breach.

for individual predictor variables applied to the GAM (Hat Island wind direction, Hat Island wind gust, GSL Breach stage, Saline and Saltair lake elevation) (Figure 15). The smoothed term plots show how discharge at the GSL Breach is influenced by each variable individually without the influence of the other variables.

Wind gusts (Figure 15a) measured at the Hat Island weather station show that when wind speeds begin to exceed 10 m/s that the discharge at the GSL Breach begins to increase in magnitude. This was observed in the April case study when wind gust exceeded 10 m/s, resulting in both increase positive flow events at the GSL Breach and the negative discharge peak occurring during the FRE.

Wind direction (Figure 15b) measured at the Hat Island weather station shows that when wind is from 0 to 60 degrees and 300 to 360 degrees (northeast to northwesterly directions), discharge at the GSL Breach is predicted by the GAM as a negative discharge event or FRE. In contrast, positive discharge events are predicted by the GAM when wind direction ranges from 60 to 300 degrees, with a greater increase in discharge when wind direction is from 180 to 220 degrees (south to southwesterly direction).

Lake water surface elevation from Saline (Figure 15c) and Saltair (Figure 15d) show a contrasting response to discharge when lake elevations increase. As elevation increases at Saline, discharge at the GSL Breach decreases until the elevation of Saline reaches an elevation of 1279 m; at an elevation of 1279 m, discharge values are negative (north-to-south flow), indicating a FRE at the GSL Breach. In contrast, as elevation at Saltair increases, discharge at the GSL Breach increases in the positive direction (south-to-north flow).

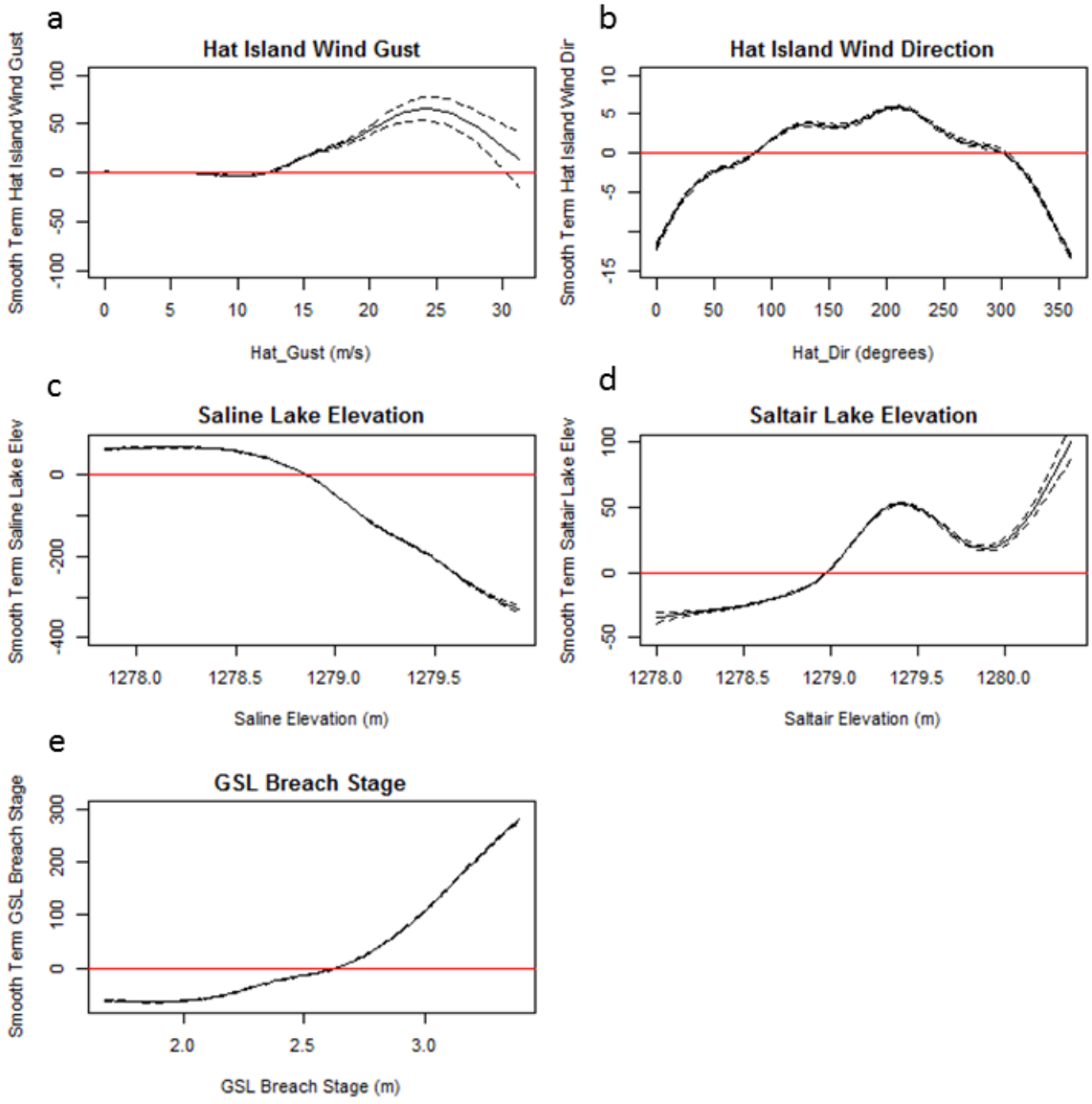

Figure 15. Smoothed term plots of predictor variables a) Hat Island wind gust, b) Hat Island wind direction, c) Saline lake elevation, d) Saltair lake elevation, and e) GSL Breach stage applied to model GH10

Stage (Figure 15e), measured at the GSL Breach gauging station, shows a similar trend as the Saltair smoothed term plot. Stage at the GSL Breach is measured on the south side of the railroad causeway and thus provides an indirect measurement of lake elevation at the GSL Breach. As stage increase at the GSL Breach discharge also increases based on the smoothed term plots.

4.4.2 Predictive Discharge Contour Maps

The smoothed term plots show the smoothing spline relationship of individual variables and how discharge is affected based on the changing conditions. The additive portion of a GAM combines the predictor variables creating a unique relationship between the variables applied to the GAM. By combining numerous predictive variables into the GAM, predictive contour maps can be generated. Figures 16 through 18 are visual summaries of how predictor variables can be used as a tool to provide an estimated discharge at the GSL Breach using the GAM method. The visual summaries are schematic contour maps that demonstrate how changing conditions of the predictor variables influence discharge at the GSL Breach. As indicated in the GAM statistical summaries, the accurate prediction of discharge at the GSL Breach requires the following variables at a minimum: wind speed or gust, wind direction, and lake water surface elevations from the Saltair and Saline gauges. Due to the multiple predictor variables needed to accurately predict discharge at the GSL Breach and the dynamic conditions observed across the lake, it is difficult to account for all variables in the visual contour maps. Due to these limitations, stream stage from the GSL Breach was not used as a predictor variable in the visual contour maps. Thus model GH7 was used for the

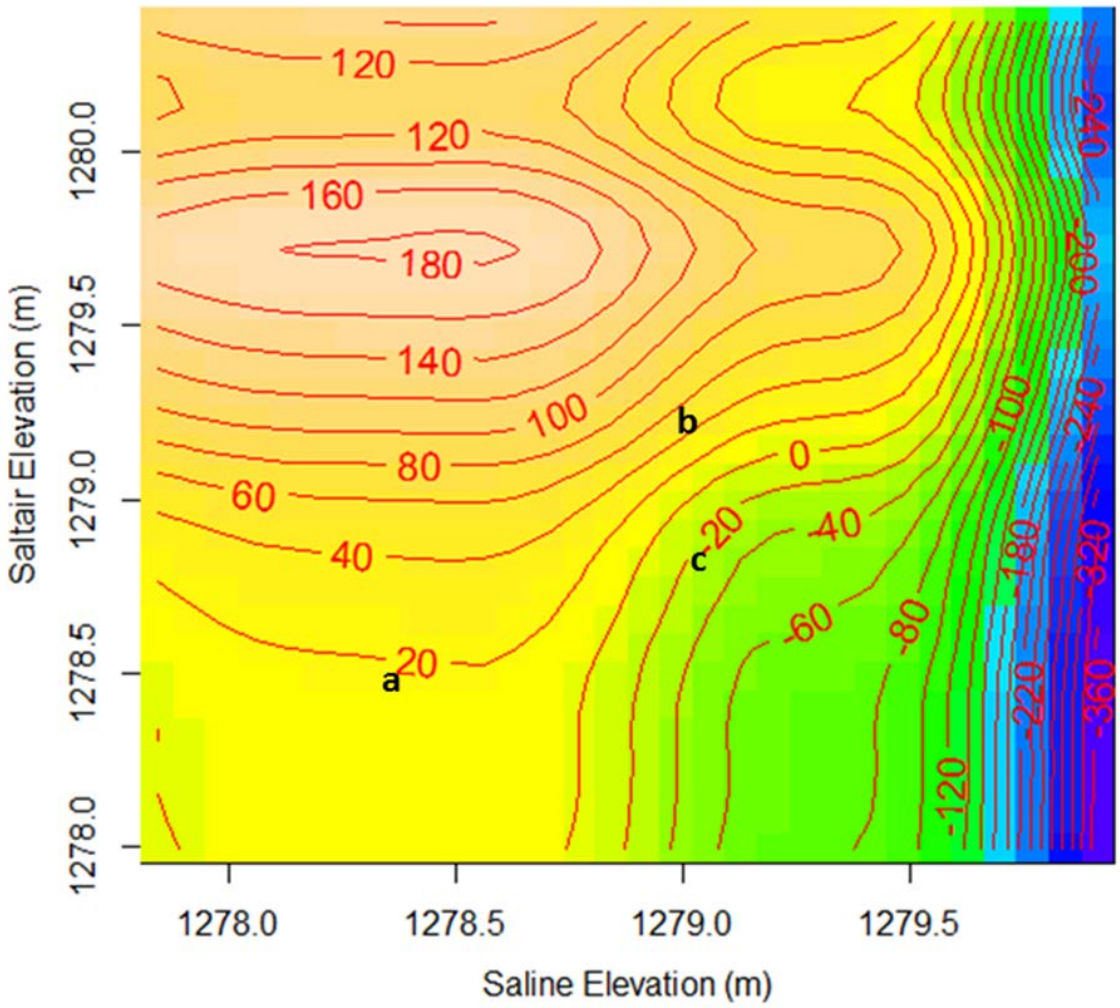

Figure 16. Predictive discharge contour map demonstrating how lake water surface elevation at Saltair and Saline influence the magnitude of discharge at the GSL Breach. Points 'a', 'b', and 'c' represent points on the contour map that are influenced by lake elevation using the GP7 model. Wind speed (0 m/s) and wind direction (180 degrees) are held constant and lake elevation varies at point 'a' (Saltair = 1278.5 m, Saline = 1278.4 m), point 'b' (Saltair = 1279.2 m, Saline = 1279.0 m), and point 'c' (Saltair = 1278.8 m, Saline = 1279.0 m). The corresponding discharge for points 'a', 'b', and 'c' are 15.7 m^3/s, 44.4 m^3/s, and -20.3 m^3/s, respectively.

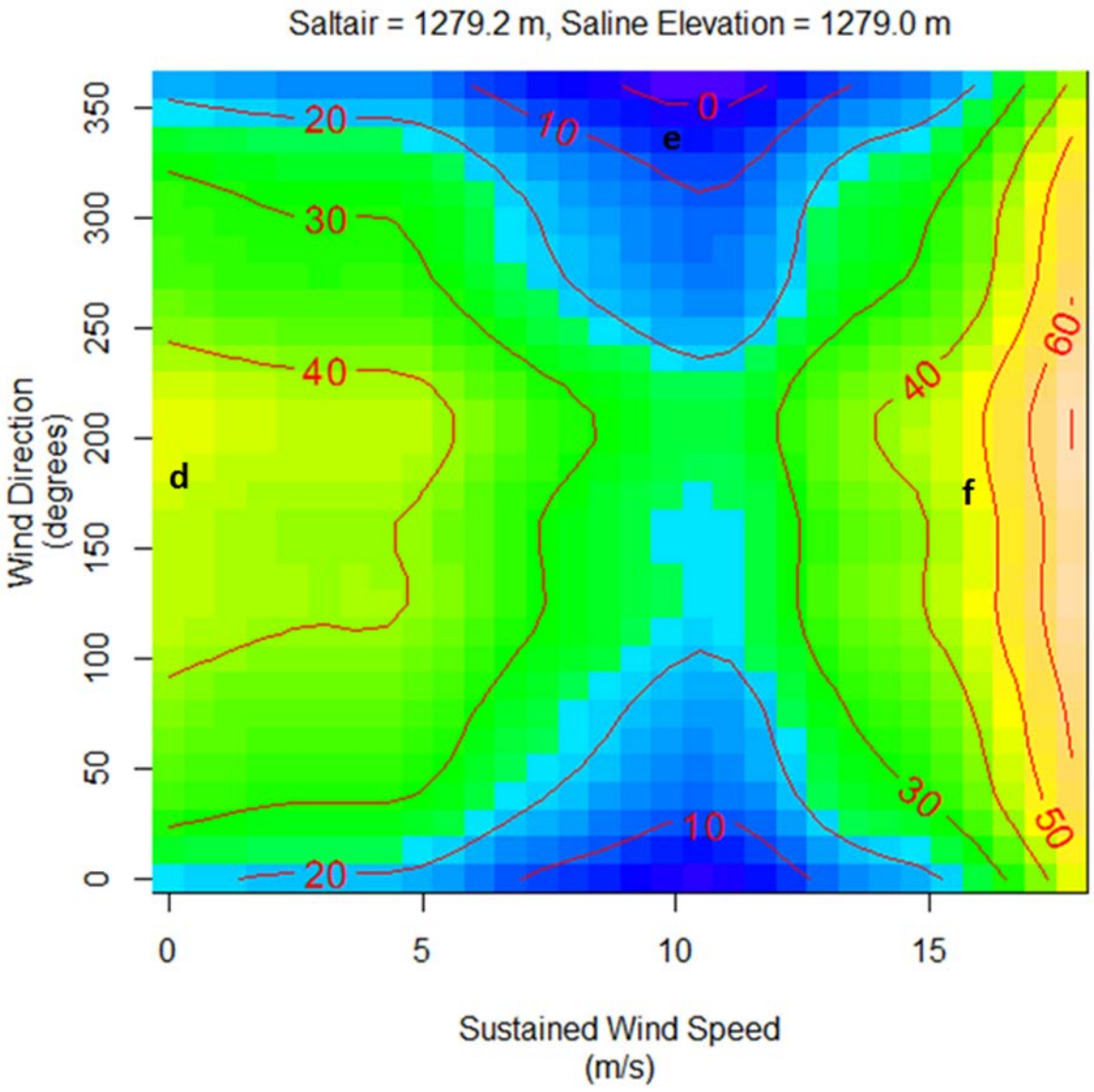

Figure 17. Predictive discharge contour map demonstrating how wind speed and wind direction influence the magnitude and flow direction of discharge at the GSL Breach. Points 'd', 'e', and 'f' represent points on the contour map that are influenced at various wind speeds and directions using the GP7 model. Lake water surface elevations at Saltair (1279.2 m) and Saline (1279.0 m) are held constant and wind speed and wind direction vary at point 'd' (wind speed = 0 m/s, wind direction = 180°), point 'e' (wind speed = 10 m/s, wind direction = 345°), and point 'f' (wind speed = 16 m/s, wind direction = 180°). The corresponding discharge for points 'd', 'e', and 'f' are 44.4 m^3/s, 2.2 m^3/s, and 47.7 m^3/s, respectively.

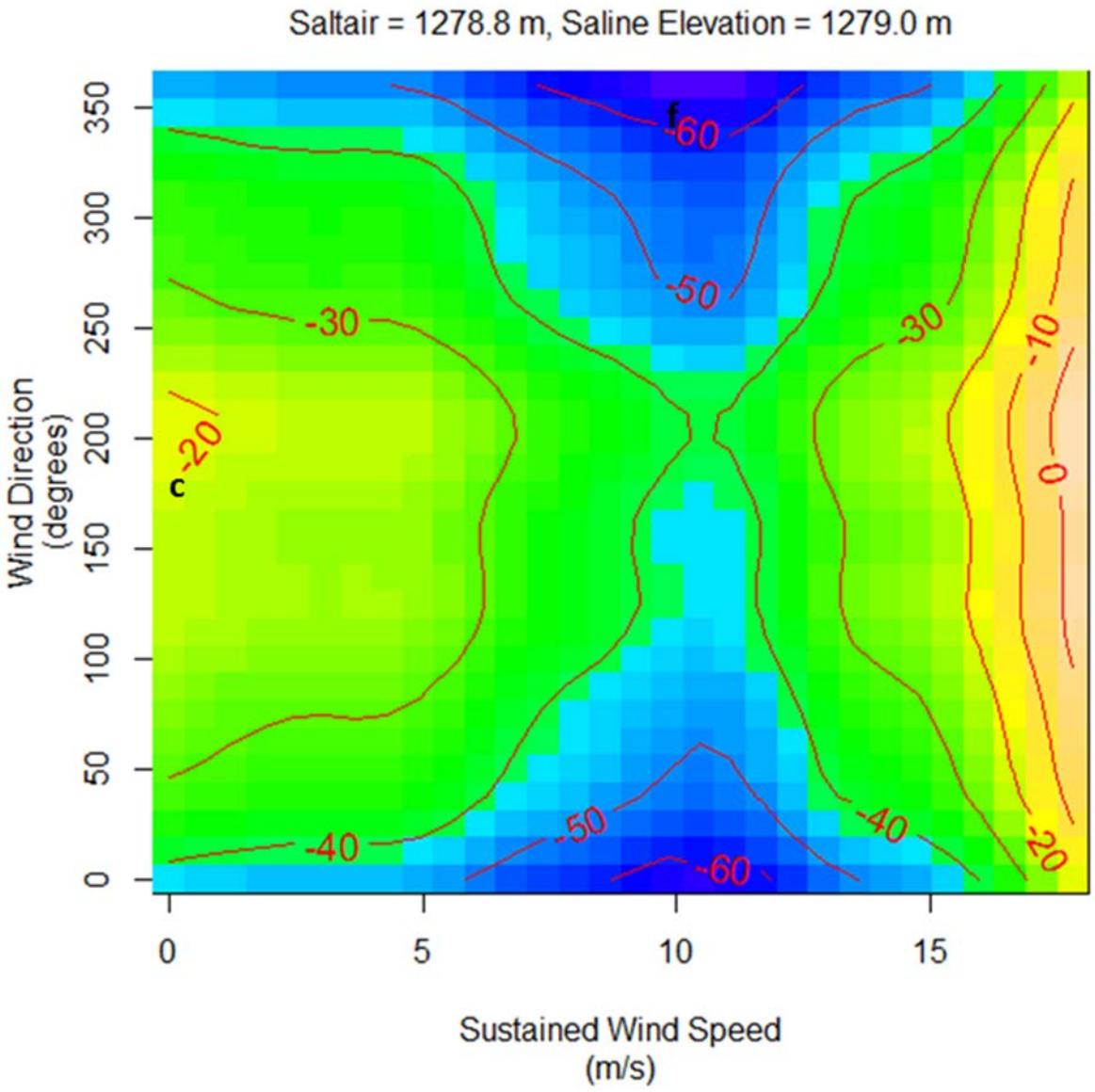

Figure 18. Predictive discharge contour map demonstrating how wind speed and wind direction influence the magnitude and flow direction of discharge at the GSL Breach. Point 'c' represent similar lake elevation conditions examine in Figure 14. Points 'c' and 'f' represent points on the contour map that are influenced at various wind speeds and directions using the GP7. Lake water surface elevations at Saltair (1278.8 m) and Saline (1279.0 m) are held constant, representing FRE conditions at the GSL Breach. Wind speed and wind direction vary at point 'c' (wind speed = 0 m/s, wind direction = 180°), and point 'g' (wind speed = 10 m/s, wind direction = 345°). The corresponding discharge for points 'c' and 'g' are -20.3 m^3/s and -60.6 m^3/s, respectively.

predictive discharge contour maps presented in Figures 16 through 18. These three contour maps are used to demonstrate how discharge at the GSL Breach changes with respect to lake water surface elevations, wind speed, and wind direction.

4.4.2.1 Lake Elevation Discharge Contour Maps

The predictive discharge contour map in Figure 16 demonstrates how lake water surface elevations at Saltair and Saline influence the magnitude of discharge at the GSL Breach. Figure 16 assumes that wind speeds are calm (wind speed = 0.0 m/s) and discharge is influenced by lake water surface elevation only. The magnitude of discharge is determined by the difference in lake water surface elevations measured at Saltair and Saline. As indicated earlier, the lake water surface elevation of Saltair (Gilbert Bay) is generally 0.06 to 0.2 m higher than the water surface elevation of Saline (Gunnison Bay). However, differences in lake water surface elevations between Saltair and Saline range between 1.04 to -0.43 m over the course of the 5-year study period.

As previously mentioned, discharge at the GSL Breach is predominately controlled by the hydrologic head difference between Saltair and Saline. Therefore, when using lake water surface elevations in Figure 16 to predict discharge at the GSL Breach, the elevation of Saltair should be greater than the elevation of Saline. In Figure 16, point ‘a’ has an elevation of 1278.5 m at Saltair and an elevation of 1278.4 m at Saline, resulting in a 0.1 m difference in water surface elevation between the two bays. The 0.1 m head difference between the two bays represents hydrologic conditions occurring in late summer when the difference in water surface elevation is lower due to evaporation and when water is diverted from the GSL tributaries reducing inflow to the

GSL. At the lake water surface elevations described for point 'a', using model GH7 (holding wind speed at 0.0 m/s and wind direction at 180 degrees constant), the predicted discharge at the GSL Breach would be approximately 15.7 m^3/s.

In Figure 16, point 'b' has an elevation of 1279.2 m at Saltair and an elevation of 1279.0 m at Saline, resulting in a 0.2 m difference in lake water surface elevation between the two bays. The 0.2 m head difference between the two bays is representative of hydrologic conditions during the spring months when discharge into the GSL is high from snowmelt runoff. The increase in hydrologic head between Gilbert and Gunnison Bay and the higher lake water surface elevations result in a higher discharge volume at point 'b', 44.4 m^3/s. In comparison, point 'c' has an elevation of 1278.8 m at Saltair and an elevation of 1279.0 m at Saline, resulting in a -0.2 m difference in water surface elevation between the two bays. This condition represents a storm seiche that displaces the water of GSL causing a change in the hydrologic head gradient. The higher water surface elevation of Saline changes the prevailing flow direction across the GSL Breach, resulting in a FRE (north-to-south flow). The FRE event is represented at point 'c' by a discharge of -20.3 m^3/s.

As lake water surface elevation increases within GSL, the magnitude of discharge at the GSL Breach increases. This is demonstrated in Figure 16 when viewing the discharge values at points 'a' and 'b'. Point 'b' has a higher discharge value and occurs at a lake elevation that is 0.7 m higher than point 'a'. The increase in discharge at a higher lake elevation is the result of an increase in cross-sectional area at the GSL Breach. At higher lake water surface elevations, a greater cross-sectional area exists, resulting in a larger volume of water flowing across the GSL Breach. In contrast, at

lower lake water surface elevations, the cross-sectional area at the GSL Breach is lower, resulting in smaller volumes of water moving across the GSL Breach. The cross-sectional area is determined by the stream stage height measured at the GSL Breach gauging station. Stream stage measured at the GSL Breach provides an approximate lake water surface elevation measured at the Saltair gauge (Gilbert Bay), which is presented in Table 4.

Discharge is computed using equation 2:

$$Q = V * A$$

where Q = discharge volume, V = water velocity, and A = cross-sectional area. If the average water velocity measured by the ADVM at the GSL Breach is 0.5 m/s and lake stage is 1.80 m (Saltair elevation approximately 1278.3 m), the cross-sectional area at the GSL Breach, taken from Table 4, would be 33.8 m^2, resulting in a discharge at the GSL Breach of 16.9 m^3/s. If lake stage increased by one meter (2.80 m, Saltair elevation approximately 1279.3 m), the cross-sectional area would be 98.6 m^2. Assuming that stream velocity did not change (0.5 m/s), discharge at the GSL Breach would be 49.3 m^3/s, which is approximately three times greater than the discharge at a stage of 1.80 m.

4.4.2.2 Wind Direction and Magnitude Discharge Contour Maps

In Figure 17, predictor variables wind speed and wind direction are introduced to the predictive discharge contour maps while holding lake water surface elevations at Saltair and Saline constant. Figure 17 maintains the same lake water surface elevations at Saltair and Saline as represented at point 'b' in Figure 16 (Saltair = 1279.2 m, Saline 1279.0 m). As wind speeds begin to increase above 5 m/s from a northerly direction (0-

Table 4.
GSL Breach stage, Saltair lake water surface elevation, and corresponding cross-sectional area measured at the GSL Breach gauging station. Cross-sectional area is based on stream stage and lake water surface elevation measured at Saltair gauging station.

Stream Stage at GSL Breach (m)	Saltair Lake Water Surface Elevation (m)	Cross-Sectional Area of GSL Breach (m^2)
1.00	1277.5	0.19
1.10	1277.6	1.07
1.20	1277.7	3.52
1.30	1277.8	7.31
1.40	1277.9	12.0
1.50	1278.0	17.1
1.60	1278.1	22.5
1.70	1278.2	28.2
1.80	1278.3	33.8
1.90	1278.4	39.7
2.00	1278.5	45.7
2.10	1278.6	51.9
2.20	1278.7	58.5
2.30	1278.8	65.0
2.40	1278.9	71.7
2.50	1279.0	78.4
2.60	1279.1	85.2
2.70	1279.2	92.0
2.80	1279.3	98.6
2.90	1279.4	105.4
3.00	1279.5	112.3
3.10	1279.6	119.2
3.20	1279.7	126.1
3.30	1279.8	133.0
3.40	1279.9	139.8
3.50	1280.0	146.8
3.60	1280.1	153.8
3.70	1280.2	160.9
3.80	1280.3	168.0
3.90	1280.4	174.9
4.00	1280.5	182.0
4.10	1280.6	189.2

30 and 330 to 360 degrees), discharge values begin to decrease in magnitude based on the direction and the magnitude of the wind speed. For example, point 'd' is represented by calm wind conditions (wind speed = 0.0 m/s, wind direction = 180 degrees) whereas point 'e' represents wind speeds of 10 m/s from a northwest direction (345 degrees). The discharge observed between points 'd' and 'e' changes considerably from 44.4 m^3/s (point 'd'), observed during calm conditions, to 2.2 m^3/s ('point 'e') during a northerly wind event. In contrast, as sustained wind speeds begin to exceed 15 m/s from a southerly direction (120 to 220 degrees), discharge values at the GSL Breach increase in the south-to-north direction, as observed at point 'f' (discharge = 47.7 m^3/s).

In Figure 18, lake water surface elevations for the discharge contour map represent the conditions examined at point 'c' in Figure 16 (Saltair = 1278.8 m, Saline = 1279.0 m). The lake water surface elevation represents conditions that would be expected during a FRE. The lake water surface elevation of Saline is greater than the elevation of Saltair, resulting in a hydrologic head gradient flowing from north-to-south. In Figure 18, the effects of wind speed and wind direction decrease discharge at the GSL Breach observed at point 'f' (discharge = -60.6 m^3/s) when wind speed (10m/s) from a northwest direction (345 degrees) is introduced to the conditions influencing discharge at the GSL Breach. The discharge at point 'f' is three time greater than the discharge at point 'c', when wind speed is calm (wind speed = 0.0 m/s), demonstrating the influence of wind on the magnitude of discharge during a FRE at the GSL Breach.

Observations derived from the predictive contour maps confirm the hypothesis and observations in the case study that southerly wind events increase discharge, whereas northerly wind events result in FRE at the GSL Breach. The predictive discharge contour

maps in Figure 17 suggest that wind speeds from a southerly direction (120 to 220 degrees) that exceed 12 m/s can double the discharge at the GSL Breach when compared to conditions when winds speeds are calm (0 to 2 m/s). As wind speed increase to 5 m/s or greater from a southerly direction, the southern fetch (65 km) increases wind shear over the length of Gilbert Bay, and "pushes" water northward up against the GSL causeway. At the same time, the water in Gunnison Bay is pushed to the northern reaches of Gunnison Bay, away from the GSL Breach, further increasing the head difference between Gilbert and Gunnison Bay at the GSL causeway.

Northerly wind events have similar results to southerly wind events across the GSL Basin. As wind speeds increase to 5 m/s or greater from a northern direction, the northern fetch (47 km) increases the effect of wind shear over Gunnison Bay, pushing water southward up against the GSL causeway. The water of Gilbert Bay is pushed south to the southern reaches of Gilbert Bay away from the GSL causeway, increasing the head difference between Gunnison and Gilbert Bay at the GSL causeway. Due to the location of the Saline and Saltair lake gauges, the lake water surface elevations at the GSL causeway is not accurately represented by the lake gauges. Both gauges respond to wind events in a similar manner as the gauges are both located in the southern portions of the individual bays in Figure 1.

4.5 Generalized Additive Model Limitation and Improvements

To improve the accuracy of predicting discharge across the GSL Breach using GAM methods, additional infrastructure is recommended to improve data collection for use within the statistical model. Since GAMs are data-driven models, quality data

collection is crucial. As observed in the residual plots and the time-series analysis, the GAM method is an accurate method of predicting discharge at lower lake elevations and discharge volumes across the GSL Breach. As lake level increases and discharge volumes increase at the GSL Breach, uncertainty in the modeled discharge values increases. The uncertainty at high discharge volumes is a result of limited calibration points at these higher flows. Therefore to improve accuracy of predicted discharge values using the GAM method, a full range of data points is needed to accurately predict discharge.

Additional weather stations along the GSL are needed to accurately measure meteorological conditions occurring over the lake. A weather station monitoring wind speed or wind gust and wind direction at the GSL Breach or in the middle of the GSL causeway would provide accurate weather conditions along the causeway and likely improve model results. While Hat Island weather station provides the best meteorological data along the lake, it is possible that southerly winds are compromised at Hat Island due to the potential wind shadow from the Oquirrh and Stansbury mountain ranges located south of Hat Island.

Additional lake water surface elevation sensors and/or stream stage sensors closer to the GSL Breach are also needed to accurately determine the hydrologic head gradient on the north and south sides of the GSL causeway. The location of existing lake gauging stations is insufficient for acquiring lake water surface elevation data during storm events. Placement of lake elevation gauges or stage sensors on the north and south side of the GSL Breach would improve the accuracy of determining the head difference between the two bodies of water, improving the accuracy of predicted discharge values

using GAM methods. The construction of a new causeway breach to replace to preexisting culvert should consider the benefits of having stage sensor on both the north and south side of the causeway.

4.6 Generalized Additive Model Implications

GAM results in this study show that accurate discharge predictions can be made when combining hydrological and meteorological data sets. The effective computation of discharge using the GAM method provides a cost-effective approach to gauging station techniques. Installation, maintenance, and long-term operation of hydroacoustic instrumentation used to measure discharge is costly, not only in GSL, but in other breach systems throughout the world. Using the methods introduced in this paper, a GAM can be produced with a shorter term gauging station installation. Once the GAM has been developed, the costly hydroacoustic instrumentation can be removed and reasonable discharge values can be predicted using less costly and easier to maintain instrumentation (i.e., stage/elevation sensors and anemometers). Some data resolution may be lost, but perhaps this could be justified by the data needs and cost savings of the funding organization.

Additional verification of the GAM method is possible in other locations along the GSL and around the world. The Farmington Bay Outflow gauging station, located on the automotive causeway separating Farmington Bay and Gilbert Bay of the GSL, offers another location that experiences similar conditions at the GSL Breach. The GAM method could also prove to be an effective approach for quantifying discharge volumes across the automotive causeway of Lake Urmia and within the Kulandy Channel of the Aral Sea. By applying the GAM methods to these systems, discharge values can be

computed to determine chemical loading potential and changes to the water and salt balance of these systems.

5. CONCLUSIONS

The GSL Breach gauging station provides a high frequency dataset of dynamic flow conditions that are observed across the GSL causeway. Flow from south-to-north, (positive flow) measured at the GSL Breach gauging station, is the predominate flow direction at the GSL Breach. However, discharge data collected at the GSL Breach show frequent changes in flow direction, reporting flow as a negative discharge value (north-to-south flow). These negative flow events are identified as FRE. As shown in this study, FREs occur throughout the year at the GSL Breach causeway and vary in frequency and duration depending on the season. During the 5-year study period (WY2009-2013), 1510 FREs were identified, and events ranged in duration from 15 minutes to 1950 minutes. FREs are most common during the timeframe of September through December; however, these FREs are short in duration, lasting less than 60 minutes. The high frequency of FREs in September through December is a result of a smaller difference in lake water surface elevations between Gilbert and Gunnison bays. FREs from January to August occur less frequently; however, the duration of the FREs is longer, with the average duration exceeding 150 minutes. FREs that occur between February and May relate to the passage of storm systems across the Great Basin region; as the front passes, a shift to strong northerly winds affects the GSL basin. These storm systems last from hours to days, causing prolonged FREs at the GSL Breach.

The analysis of a FRE event that occurred in April of 2010 suggests that during

southerly winds, the lake elevation gauging stations of Saline and Saltair both show a drop in lake elevation as water is displaced to the northern reaches of Gunnison and Gilbert Bay. As water is displaced to the north by the southern wind, stage at the GSL Breach increases the hydrologic head gradient at the GSL Breach. This coincides with an increase in discharge from a positive direction (south-to-north flow) across the GSL Breach. Northerly winds displace water to the southern reaches of the Gunnison and Gilbert bays, causing the lake elevation gauges of Saline and Saltair to both increase in lake elevation. During this time, stage decreases at the GSL Breach, suggesting that the hydrologic head gradient has switched and the head gradient is greater to the north of the GSL causeway. This results in a negative discharge event (north-to-south flow) or a FRE.

GAMs produced in this study used measured parameters from hydrologic and meteorological stations to model discharge at the GSL Breach on the GSL causeway. A minimum of four predictor variables (wind gust, wind direction, lake water surface elevation from Saline and Saltair lake gauging stations) are needed to accurately compute discharge at the GSL Breach. The deviance explained when applying these four variables to a GAM is approximately 65 percent. However, five predictor variables are ideal for predicting discharge at the GSL Breach. The five predictor variables include; 15-minute wind gusts, wind direction, lake water surface elevation from Saltair and Saline gauges and stream stage collected at the GSL Breach gauging station. The deviance explained when applying these five variables to a GAM is approximately 75 percent. Of the two weather stations used in this analysis, meteorological data collected at Hat Island station resulted in higher confidence in the computed discharge values of models GH9 and GH10. Discharge values derived using the GAM methods were biased low when

modeled discharge values exceeded 50 m^3/s and when discharge values dropped below 0 m^3/s. Modeled discharge values were generally lower in magnitude for both positive and negative discharge events.

Time-series comparisons of both observed and modeled discharge values show that modeled discharge values simulate the abrupt changes in discharge that are common at the GSL Breach. This suggests that the sensitivity of the GAM is sufficient in modeling the resolution of timing and magnitude of discharge at the GSL Breach. This provides a useful tool for understanding the key variables that influence the hydrodynamics of the GSL.

The application of the GAM method to the hydrologic and metrological dataset provides numerous tools that can be used to predict discharge at the GSL Breach. Predictive discharge contour maps, produced from the GAM results, can be used as predictive tools for determining discharge across the GSL Breach using specified variables. Smoothed term plots and predictive discharge contour maps confirm that northerly winds result in reduced positive flows or FRE events across the GSL Breach. Predictive discharge contour maps indicate that when wind speeds begin to exceed 5 m/s from a northerly direction (0-30 and 330 to 360 degrees), discharge decreases and/or FREs occur across the GSL Breach. In contrast, winds speeds that begin to exceed 10 m/s from a southerly direction (150 to 210 degrees) increase discharge for positive discharge events (south-to-north) at the GSL Breach.

The magnitude and direction of the wind affects the difference in lake water surface elevation at the gauging station, influencing the magnitude and direction of flow direction at the GSL Breach. The location of the Saltair and Saline lake gauges do not

accurately measure the lake water surface elevation differences observed at the GSL Breach. However, stream stage measured at the GSL Breach acts as an indirect measure of the lake water surface elevation suggesting the direction of the hydrologic head gradient at the causeway which influences the flow direction at the GSL Breach. The addition of lake water surface elevation sensors or stage sensors located on both the north and the south side of the GSL causeway would eliminate assumptions of hydrologic head gradients influencing flow across the GSL causeway. This would verify that the elevation of Gunnison Bay needs to exceed the elevation of Gilbert Bay to result in a FRE at the GSL Breach.

Monitoring and managing the waters of GSL has become a greater priority for extractive industries, scientists, resource managers, and regulating officials. Results of this study provide a baseline for understanding the hydrodynamic variables affecting discharge at the GSL Breach. FREs associated with passing frontal weather systems at the GSL Breach deliver large volumes of deep brine water into Gilbert Bay as a result of northerly wind shear. These reversal events typically last less than a couple hours, but have the ability to distribute large volumes of concentrated brine from Gunnison Bay into Gilbert Bay, which might adversely impact the functionality of the lake ecosystems. Calculations by Naftz et al. (In Press) suggests that one of these reversal events at the GSL Breach has the ability to discharge more dissolved solids into Gilbert Bay than the total annual load of dissolved solids from the Bear River by almost two orders of magnitude. Assessing the new data collected across the GSL is valuable for understanding the lake hydrodynamics in context of the many changes currently affecting the state of the lake and its circulation. The data collected at the GSL Breach provides

insight to the hydrodynamics influencing flow across the GSL causeway and should be considered during the planning stages of a replacement breach.

The closure of culverts on the GSL causeway and the potential construction of a new causeway underscore the importance of understanding the many parameters and variables that influence lake hydrodynamics. Our study demonstrates the utility of modeling applications that may be deployed for assessments of GSL circulation, flow forecasting, and in development test scenarios for environmental and hydrological management decisions. Potentially important variables that can be modeled at a regional and seasonal scale might include any natural or anthropogenic activities that affect water volumes and lake elevation, including storms, extreme weather events, floods, runoff inputs, influent stream water divertments, irrigation, regional drought severity, earthwork constructions, dredging, mineral extractions, and effluent discharges by industry.

REFERENCES

Akaike, H., 1973. Information theory as an extension of the maximum likelihood principle. In: Petrov, B.N., Csaki, F. (Eds.), Second International Symposium on Information Theory. Akademiai Kiado, Budapest, Hungary, pp. 267-28.

Alcott, T.I., Steenburgh, W.J., 2013. Orographic influences on a Great Salt Lake-effect snowstorm. Monthly Weather Review, 141(7): 2432-2450.

Alcott, T.I., Steenburgh, W.J., Laird, N.F., 2012. Great Salt Lake-effect precipitation: Observed frequency, characteristics, and associated environmental factors. Weather and Forecasting, 27(4): 954-971.

Aldrich, T.W., Paul, D.S., 2002. Avian ecology of Great Salt Lake. Great Salt Lake: An Overview of Change. Special publication of the Utah Department of Natural Resources, Salt Lake City, Utah: 343-374.

Arnow, T., Stephens, D.W., 1990. Hydrologic characteristics of the Great Salt Lake, Utah, 1847-1986. U.S. Geological Survey Water-Supply Paper, 2332: 1-32.

Asquith, W.H., Herrmann, G.R., Cleveland, T.G., 2013. Generalized Additive Regression Models of Discharge and Mean Velocity Associated with Direct-Runoff Conditions in Texas: Utility of the U.S. Geological Survey Discharge Measurement Database. Journal. of Hydrologic Engineering, 18(10): 1331-1348.

Associated Press, 2013. Culvert in Great Salt Lake causeway in peril, Daily Herald. 11November 2013. http://www.heraldextra.com/news/state-and-regional/culvert-in-great-salt-lake-causeway-in-peril/article_b68652b2-2a9c-569a-b8ea-3ce12406dd9d.html.

Atwood, G., 2002. Storm-Related Flooding Hazards, Coastal Processes, and Shoreline Evidence of Great Salt Lake. Great Salt Lake: An Overview of Change. Special Publication of the Utah Department of Natural Resources, Salt Lake City, Utah: 44-53.

Augustin, N.H., Borchers, D.L., Clarke, E.D., Buckland, S.T., Walsh, M., 1998. Spatiotemporal modelling for the annual egg production method of stock assessment using generalized additive models. Canadian Journal of Fisheries and Aquatic Sciences, 55(12): 2608-2621.

Beal, L.M., Molinari, R.L., Chereskin, T.K., Robbins, P.E., 2000. Reversing bottom circulation in the Somali Basin. Geophysical Research Letters, 27(16): 2565-2568.

Beisner, K., Naftz, D.L., Johnson, W.P., Diaz, X., 2009. Selenium and trace element mobility affected by periodic displacement of stratification in the Great Salt Lake, Utah. Science of the Total Environment, 407(19): 5263-5273.

Bioeconomics Inc., 2012. Economic Significance of the Great Salt Lake to the State of Utah. Prepared for the Great Salt Lake Advisory Council. January 26, 2012.

Carling, G.T., Fernandez, D.P., Rudd, A., Pazmino, E., Johnson, W.P., 2011. Trace element diel variations and particulate pulses in perimeter freshwater wetlands of Great Salt Lake, Utah. Chemical Geology, 283(1-2): 87-98.

Diaz, X., Johnson, W.P., Fernandez, D., Naftz, D.L., 2009a. Size and elemental distributions of nano- to micro-particulates in the geochemically-stratified Great Salt Lake. Applied Geochemistry, 24(9): 1653-1665.

Diaz, X., Johnson, W.P., Naftz, D.L., 2009b. Selenium mass balance in the Great Salt Lake, Utah. Science of the Total Environment, 407(7): 2333-2341.

Dicataldo, G. et al., 2011. Diel variation of selenium and arsenic in a wetland of the Great Salt Lake, Utah. Applied Geochemistry, 26(1): 28-36.

Elken, J., Raudsepp, U., Lips, U., 2003. On the estuarine transport reversal in deep layers of the Gulf of Finland. Journal of Sea Research, 49(4): 267-274.

Ferrarin, C., Umgiesser, G., 2005. Hydrodynamic modeling of a coastal lagoon: The Cabras lagoon in Sardinia, Italy. Ecological Modelling, 188(2-4): 340-357.

Ghezzo, M., Guerzoni, S., Cucco, A., Umgiesser, G., 2010. Changes in Venice Lagoon dynamics due to construction of mobile barriers. Coastal Engineering, 57(7): 694-708. Gianni, A., Kehayias, G., Zacharias, I., 2011. Geomorphology modification and its impact to anoxic lagoons. Ecological Engineering, 37(11): 1869-1877.

Gianni, A., Zacharias, I., 2012. Modeling the hydrodynamic interactions of deep anoxic lagoons with their source basins. Estuarine, Coastal and Shelf Science, 110: 157-167.

Guisan, A., Edwards Jr, T.C., Hastie, T., 2002. Generalized linear and generalized additive models in studies of species distributions: setting the scene. Ecological Modelling, 157(2–3): 89-100.

Gwynn, J.W., 2002. Great Salt Lake, Utah: Chemical and physical variations of the brine and effects of the SPRR causeway, 1966-1996. Great Salt Lake: An Overview of Change. Special Publication of the Utah Department of Natural Resources, Salt Lake City, Utah: 87-106.

Gwynn, J.W., 2012. A lake divided—a history of the Southern Pacific Railroad causeway and its effect on Great Salt Lake, Utah. <http://geology.utah.gov/utahgeo/gsl/lakedivided.htm>.

Hahl, D.C., Handy, A.H., 1969. Chemical and physical variations of the brine, Great Salt Lake, Utah, 1963-1966. Utah Geological Survey Water Resource Bulletin, 12: 1-33.

Hahnenberger, M., Nicoll, K., 2012. Meteorological characteristics of dust storm events in the eastern Great Basin of Utah, U.S.A. Atmospheric Environment, 60: 601-612.

Hahnenberger, M., Nicoll, K., 2014. Geomorphic and land cover identification of dust sources in the eastern Great Basin of Utah, U.S.A. Geomorphology, 204: 657-672.

Hamblin, P.F., He, C., 2003. Numerical models of the exchange flows between Hamilton Harbour and Lake Ontario. Canadian Journal of Civil Engineering, 30(1): 168-180.

Hastie, T.J., Tibshirani, R.J., 1990. Generalized Additive Models. Chapman & Hall/CRC Press.

Ilicak, M., Özgökmen, T.M., Peters, H., Baumert, H.Z., Iskandarani, M., 2008. Very large eddy simulation of the Red Sea overflow. Ocean Modelling, 20(2): 183-206.

Jacobs Associates, 2013. Great Salt Lake Causeway East Culvert - Results of Diving Inspection, 11 October 2013. http://www.waterquality.utah.gov/PublicNotices/docs/2013/UPRRCauseway/UPRRJAGSLEastCulvertStatusMemo1021132.pdf.

Jia, P., Li, M., 2012a. Circulation dynamics and salt balance in a lagoonal estuary. Journal of Geophysical Research C: Oceans, 117(1).

Jia, P., Li, M., 2012b. Dynamics of wind-driven circulation in a shallow lagoon with strong horizontal density gradient. Journal of Geophysical Research C: Oceans, 117(5).

Johnson, K.K., Loving, B.L., 2002. Use of an Acoustic Doppler Current Profiler (ADCP) to Measure Hypersaline Bidirectional Discharge. Hydraulic Measurements and Experimental Methods 2002: 238-249.

Levesque, V.A., Oberg, K.A., 2012. Computing discharge using the index velocity method. U.S. Geological Survey Techniques and Methods, 3-A23: 1-148.

Lin, A., 1977. Final report on wind tides of the Great Salt Lake. Utah Geological and Mineralogical Survey.

Loving, B.L., Waddell, K.M., Miller, C.W., 2000. Water and salt balance of Great Salt Lake, Utah, and simulation of water and salt movement through the causeway, 1987–1998. U.S. Geological Survey Water-Resources Investigations Report. (2000-4221).

MacCready, P., Banas, N.S., Hickey, B.M., Dever, E.P., Liu, Y., 2009. A model study of tide- and wind-induced mixing in the Columbia River Estuary and plume. Continental Shelf Research, 29(1): 278-291.

Madison, R.J., 1970. Effects of a causeway on the chemistry of the brine in Great Salt Lake, Utah. Utah Geological Surve Water-Resource Bulletin, 14: 52.

Maffly, B., 2013a. Collapse 'imminent' for Great Salt Lake culvert on causeway, Salt Lake Tribune. 7 November 2013. http://www.sltrib.com/sltrib/news/57087689-78/lake-culvert-causeway-railroad.html.csp

Maffly, B., 2013b. Failing culvert prompts sealing of Great Salt Lake's North Arm, Salt Lake Tribune. 11 December 2013. http://www.sltrib.com/sltrib/news/57250070-78/lake-culvert-causeway-salt.html.csp

Maffly, B., 2013c. Utah fast-tracks plan to fill Great Salt Lake culvert, Salt Lake Tribune. 13 December 2013.

Marjani, A., Jamali, M., 2014. Role of exchange flow in salt water balance of Urmia Lake. Dynamics of Atmospheres and Oceans, 65: 1-16.

McCullagh, P., Nelder, J.A., 1989. Generalized Linear Models, Second Edition. Chapman & Hall, London.

Mohammed, I.N., Tarboton, D.G., 2012. An examination of the sensitivity of the Great Salt Lake to changes in inputs. Water Resources Research, 48(11).

Morton, R., Henderson, B.L., 2008. Estimation of nonlinear trends in water quality: An improved approach using generalized additive models. Water Resources Research, 44(7).

Naftz, D., Angeroth, C., Freeman, M., Rowland, R., Carling, G., 2013. Monitoring Change in Great Salt Lake. Eos, Transactions American Geophysical Union, 94(33): 289--290.

Naftz, D., Angeroth, C., Kenney, T., Waddell, B., Darnall, N., Silva, S., Perschon, C., Whitehead, J., 2008. Anthropogenic influences on the input and biogeochemical cycling of nutrients and mercury in Great Salt Lake, Utah, USA. Applied Geochemistry, 23(6): 1731-1744.

Naftz, D.L., Carling, G.T., Angeroth, C., Freeman, M., Rowland, R., Pazmino, E., In Press. Density stratified flow events in Great Salt Lake, Utah, USA: Implications for mercury and salinity cycling.

Naftz, D.L., Cederberg, J.R., Krabbenhoft, D.P., Beisner, K.R., Whitehead, J., Gardberg, J., 2011. Diurnal trends in methylmercury concentration in a wetland adjacent to Great Salt Lake, Utah, USA. Chemical Geology, 283(1-2): 78-86.

Naftz, D.L., Johnson, W.P., Freeman, M.L., Beisner, K., Diez, X., Cross, V.A., 2009. Estimation of selenium loads entering the south arm of Great Salt Lake, Utah, from May 2006 through March 2008. U.S. Geological Survey Scientific Investigations Report (2008-5069): 40.

National Climatic Data Center (NCDC), National Oceanic and Atmospheric Administration (NOAA), 2014.Climate Data Online: Dataset Discovery. http://www.ncdc.noaa.gov/cdo-web/datasets.

Oliver, W., Fuller, C., Naftz, D.L., Johnson, W.P., Diaz, X., 2009. Estimating selenium removal by sedimentation from the Great Salt Lake, Utah. Applied Geochemistry, 24(5): 936-949.

Palmer, W.C., 1965. Meteorological drought. US Department of Commerce, Weather Bureau Washington, DC, USA.

R, 2013. The R project for statistical computing. http://www.r-project.org/.

Rantz, E.S., others, 1982a. Measurement and computation of streamflow: Volume 1, Measurement of stage and discharge. U.S. Geological Survey Water Supply Paper(2175): 1-284.

Rantz, E.S., others, 1982b. Measurement and computation of streamflow: Volume 2, Computation of Discharge. U.S. Geological Survey Water Supply Paper (2175): 285-631.

Rich, J., 2002. Great Salt Lake South Arm Circulation: Currents, Velocities and Influencing Factors. Great Salt Lake: An Overview of Change. Special Publication of the Utah Department of Natural Resources, Salt Lake City, Utah: 171-183.

Roget, E., Zavialov, P., Khan, V., Muñiz, M.A., 2009. Geodynamical processes in the channel connecting the two lobes of the Large Aral Sea. Hydrology and Earth System Sciences, 13(11): 2265-2271.

Skorko, K., Jewell, P.W., Nicoll, K., 2012. Fluvial response to an historic lowstand of the Great Salt Lake, Utah. Earth Surface Processes and Landforms, 37(2): 143-156.

Smeed, D., 1997. Seasonal variation of the flow in the strait of Bab al Mandab. Oceanologica Acta, 20(6): 773-781.

Smeed, D.A., 2004. Exchange through the Bab el Mandab. Deep-Sea Research Part II: Topical Studies in Oceanography, 51(4-5): 455-474.

Spall, R.E., 2009. A hydrodynamic model of the circulation within the south arm of the Great Salt Lake. International Journal of Modelling and Simulation, 29(2): 181-190.

Ström, T.E., Klaveness, D., 2003. Hunnebotn: A seawater basin transformed by natural and anthropogenic processes. Estuarine, Coastal and Shelf Science, 56(5-6): 1177-1185.

Underwood, F.M., 2009. Describing long-term trends in precipitation using generalized additive models. Journal of Hydrology, 364(3-4): 285-297.

Union Pacific Railroad, 2013. USACE Notification re Imminent Failure of East Culvert. Union Pacific Railroad. http://www.waterquality.utah.gov/PublicNotices/docs/2013/UPRRCauseway/UPRRLtr21Oct2013USACENotificationreImminentFailureofEastCulvertFinal20131021 2.pdf

University of Utah MesoWest, 2013. MesoWest Observations and Summaries. http://mesowest.utah.edu/index.html

U.S. Geological Survey, 2013a. National Water Information System: Current Conditions for Utah: Streamflow. http://waterdata.usgs.gov/ut/nwis/current/?type=flow.

U.S. Geological Survey, 2013b. Water Watch. http://waterwatch.usgs.gov/index.php

U.S. Geological Survey, 2014. OSW Hydroacoustics: Index-Velocity Instruments. http://hydroacoustics.usgs.gov/indexvelocity/instruments.shtml

Utah Division of Forestry, Fire and State Lands, 2012. Draft Final Great Salt Lake Comprehensive Management Plan. 305.

Waddell, K.M., Bolke, E.L., 1973. The effects of restricted circulation on the salt balance of Great Salt Lake, Utah. Utah Geological Survey Water-Resource Bulletin(18): 54.

Waddell, K.M., Fields, F.K., 1977. Model for evaluating the effect of dikes on the water and salt balance of Great Salt Lake, UT. Utah Geological Survey Water-Resource Bulletin(21): 54.

Wen, L., Rogers, K., Ling, J., Saintilan, N., 2011. The impacts of river regulation and water diversion on the hydrological drought characteristics in the Lower Murrumbidgee River, Australia. Journal of Hydrology, 405(3-4): 382-391.

Wold, S.R., Thomas, B.E., Waddell, K.M., 1997. Water and salt balance of the Great Salt Lake, Utah, and simulation of water and salt movement through the causeway. U.S. Geological Survey Water-Supply Paper(2450): 64.

Wood, S.N., 2006. Generalized additive models: an introduction with R. Chapman &

Hall/CRC Press.

Wood, S.N., 2014. mgcv: GAMs with GCV/AIC/REML smoothness estimation and GAMMs by PQL, Rpackage version 1.7-6.

Wurtsbaugh, W.A., Gardberg, J., Izdepski, C., 2011. Biostrome communities and mercury and selenium bioaccumulation in the Great Salt Lake (Utah, USA). Science of the Total Environment, 409(20): 4425-4434.

Wurtsbaugh, W.A., Maciej Gliwicz, Z., 2001. Limnological control of brine shrimp population dynamics and cyst production in the Great Salt Lake, Utah. Hydrobiologia, 466: 119-132.

Yeager, K.N., James Steenburgh, W., Alcott, T.I., 2013. Contributions of lake-effect periods to the cool-season hydroclimate of the great salt lake Basin. Journal of Applied Meteorology and Climatology, 52(2): 341-362.

Zacharias, I., Gianni, A., 2008. Hydrodynamic and dispersion modeling as a tool for restoration of coastal ecosystems. Application to a re-flooded lagoon. Environmental Modelling and Software, 23(6): 751-767.

Zavialov, P.O. et al., 2003. Hydrographic survey in the dying Aral Sea. Geophysical Research Letters, 30(13): 2-1.

Zavialov, P.O., Ni, A.A., Kudyshkin, T.V., Kurbaniyazov, A.K., Dikarev, S.N., 2009. Five years of field hydrographic research in the Large Aral Sea (2002-2006). Journal of Marine Systems, 76(3): 263-271.

Zeinoddini, M., Tofighi, M.A., Vafaee, F., 2009. Evaluation of dike-type causeway impacts on the flow and salinity regimes in Urmia Lake, Iran. Journal of Great Lakes Research, 35(1): 13-22.

Zemlys, P., Ferrarin, C., Umgiesser, G., Gulbinskas, S., Bellafiore, D., 2013. Investigation of saline water intrusions into the Curonian Lagoon (Lithuania) and two-layer flow in the Klaipeda Strait using finite element hydrodynamic model. Ocean Science, 9(3): 573-584.